universität wien

# DIPLOMARBEIT

Titel der Diplomarbeit

## Characterisation of a new GEM detector with PIXE at VERA

angestrebter akademischer Grad

Magister der Naturwissenschaften (Mag. rer. nat.)


| | |
|---|---|
| Verfasser: | Philipp Müllner |
| Matrikel-Nummer: | 0202229 |
| Studienrichtung: | 411 Physik |
| Betreuer: | Ao. Univ.-Prof. DI Dr. Robin Golser |


Wien, am 6. März 2009

**Abstract**

The next generation of hadron physics experiments aims at studying rare processes with rigorous improved sensitivity (e.g. PANDA).

The technical requirements include high beam intensities, fast detectors for charged particles with large acceptance and excellent tracking capabilities. Detectors, which base on the GEM (Gas Electron Multiplier) technology, meet the demands for such experiments. GEM detectors have a high rate capability, excellent spatial-resolution, good time resolution and low material budget inside the active area in order not to spoil the mass and energy resolution of the detector. Furthermore the GEM detectors can be build with a very large active area of the order of $m^2$.

The GEM technology bases on a typically $50\,\mu m$ thick polyimide foil with a typically $5\,\mu m$ thick copper cladding on both sides. A large number of microholes with a diameter of $70\,\mu m$ and a distance of $140\,\mu m$ were chemically etched into this foils. Inside each hole an electric field, which acts as a multiplication channel for electrons, of several of $kV/cm$ is produced by applying a voltage difference of several hundred volts between both copper sides. A GEM detector is a gas detector, where one or several GEM-foils are mounted between cathode and anode.

A GEM detector, which was designed in the SMI (Stefan Meyer Institute for subatomic physics), was tested with PIXE (Proton Induced X-ray Emission) at VERA in this work. The detector was composed of a $5\,\mu m$ thick aluminum coated mylar foil, three GEM foils with a $50\,\mathrm{x}\,50\,mm^2$ active area and a readout anode, which consists of ten independent copper stripes. The location-dependence of the intrinsic efficiency and the signal amplification of the GEM detector across the detection area were measured at this work. Therefore characteristic X-rays were produced using PIXE, which were restricted to a small beam by a pinhole. The small X-ray beam excited only a small area on the GEM detector. The location independence of the efficiency and signal amplification across the detection area were determined by comparison of the data of each small area.

The data showed a high stability of the efficiency across the detection area of the GEM detector. But the signal amplification showed a location dependence across the detection area.

The data of this work will help further developments of GEM detectors and showed also the capability of PIXE for GEM detector characterisation.

## Zusammenfassung

Ein wesentlicher Teil zukünftige Hadronenexperimente gilt der Studie seltener Prozesse mit drastisch verbesserter Empfindlichkeit (z.B. PANDA). Die technischen Voraussetzungen für diese Experimente beinhalten hohe Strahl Intensitäten, schnelle Detektoren für geladene Teilchen mit großer Akzeptanz und ausgezeichneten *Tracking* Eigenschaften. Detektoren, die auf der GEM (Gas Electron Multiplier) Technologie basieren, erbringen die technischen Voraussetzung für diese Experimente. Solche GEM Detektoren haben die Eigenschaften sehr hohe Raten zu verarbeiten, eine hervorragende Ortsauflösung, eine gute Zeitauflösung und sehr wenig Deektormaterial in der aktiven Zone, um nicht Energie- bzw. Massenauflösung des Detektors zu beeinträchtigen. Eine weitere Besonderheit dieser Detektoren ist, dass die Größe der aktiven Detektorzone bis in den $m^2$ Bereich gebaut werden kann.

Die GEM Technologie basiert auf einer beidseitig kupferbeschichteten Polyimidfolie. In dieser Folie sind viele Mikrolöcher mit einem Durchmesser von typischerweise $70\,\mu m$ in einem Abstand von typischerweise $140\,\mu m$ chemisch geätzt worden. Durch Anlegen einer Spannungsdifferenz von mehreren hundert Volt zwischen den Kupferschichten wird ein elektrisches Feld von mehreren $kV/cm$ in jedem Mikroloch erzeugt, welches als Verstärker für Elektronen wirkt. Ein GEM Detektor ist ein Gasdetektor in dem zwischen Kathode und Anode eine oder mehrere GEM Folien eingebaut sind, wodurch eine Verstärkungsfaktor von $10^4$ - $10^5$ erreicht werden kann.

In dieser Arbeit wurde ein vom SMI (Stefan Meyer Institut für subatomare Physik) entwickelter GEM Detektor mittels PIXE (Proton Induced X-ray Emission) am VERA Beschleuniger getestet. Der Detektor besteht aus einer $5\,\mu m$ dicken aluminisierten Mylarfolie als Kathode, drei GEM Folien mit einer $50\,\mathrm{x}\,50\,mm^2$ großen aktiven Zone und einer Ausleseanode mit zehn seperaten Kupferstreifen. Der Detektor wurde auf seine Ortsunabhängigkeit bezüglich *intrinsic Efficiency* und Signalverstärkung geprüft. Die Aufgabe war zu ermitteln, ob die *intrinsic Efficiency* und Signalverstärkung über die Detektorfläche konstant ist. Dazu wurde mittels PIXE charakteristische Röntgenstrahlung erzeugt, die durch eine Lochblende auf einen kleinen Richtstrahl begrenzt wurde. Dieser Richtstrahl regte nur einen kleinen Teil der Detektorfläche gleichzeitig an. Die von diesen kleinen Bereichen gewonnen Daten wurden miteinader verglichen, um mögliche Abweichungen in der *Efficiency* bzw. Signalverstärkung zu ermitteln.

Zusammengefasst kann man sagen, dass die *Efficiency* des Detektors über die Detektorfläche sehr konstant ist und nur teilweise geringe Abweichungen aufweist, die auf statistische Schwankungen der Messergebnisse zurückgeführt werden können. Anders zeigte Signalverstärkung bei denMessungen eine Ortsabhängigkeit.

Die aus dieser Arbeit gewonnen Daten helfen bei der Weiterentwicklung von GEM Detektoren und zeigen auch das Potential von PIXE als mögliche Messmethode zur Charakterisierung von GEM Detektoren.

# Contents

# 1 Theory

## 1.1 PIXE - Proton Induced X-ray Emission

Proton Induced X-ray Emission, short PIXE, is a nondestructive method for material element analysis. PIXE bases on the production of characteristic X-rays, which are unique for each element, by ionizing the atoms of a specimen due to Coulomb interaction with protons. The biggest advantage of PIXE is that it can be performed on air, which gives the possibility to analyse precious art objects.

### 1.1.1 Protons in matter

When protons fly through matter, they interact with the target atoms by ionizing them due to collision with the electrons. Because of the ionization of the atoms the protons suffer an energy loss. This energy loss $dE_1$ of the protons per path unit $dx$ in matter can be calculated with the Bethe-Bloch-formula (see formula 1.1).

$$-\frac{dE_1}{dx} = \frac{4\pi Z_1^2 e^4}{m_e v_1^2 (4\pi\epsilon_0)^2} \cdot Z_2 \cdot ln\left(\frac{2m_e v_1^2}{U}\right) \tag{1.1}$$

$E_1$, $Z_1$ and $v_1$ determines the energy, atomic number and velocity of the protons. $Z_2$ is the atomic number of the target atom. $m_e$ describes the electron mass and $U$ is the excitation potential of the target.

The relative short stopping path of protons in matter (order of $100\,\mu m$) is a limitation fact for depth-resolved analysis with PIXE.

### 1.1.2 Characteristic X-ray production

A proton produces an inner shell hole in a specimens atom and thereby ionize it. Therefore an energy, which is at least equal to the binding energy of the inner shell, has to be transfered to the ejected electron. An electron from a higher shell falls to the hole of the inner shell. The released energy, whose value is given by the difference of the binding energies between the two shells, will be emitted by sending out a photon or an electron from a higher shell, the so called Auger electron (see fig. 1.1).

The probability of a X-ray emission can be described by the fluorescence yield. The fluorescence yield is a function of the atomic number $Z$ of the target atom. The probability of X-ray emission increases with increasing $Z$ while the Auger-electron emission probability is higher for lighter elements with low $Z$.

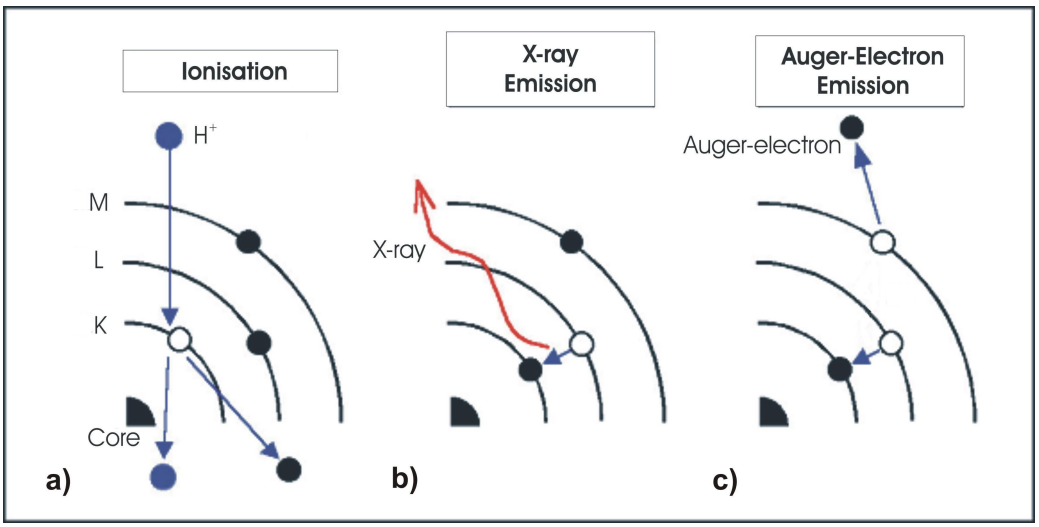


**Figure 1.1:** a) Ionisation of the target atom by $H^+$ bombardment; b)Emission of a characteristic X-ray after electron transition; c)Emission of an Auger-electron after electron transition (Figure from [Krimse, 2000])

The energy of an emitted X-ray is characteristic for each element and can be determined by Moseley's law (1.2).

$$E_Z = E_0 \cdot (Z - S)^2 \cdot \left(\frac{1}{n^2} - \frac{1}{m^2}\right) \tag{1.2}$$

The energy $E_Z$ of the emitted X-ray is proportional to the square of the atomic number $Z$ of the atom. The parameter $S$ is the so called shielding constant, which defines the shielding of the core charge through other electrons.For K-lines (n=1) it is about 1.0 and for L-lines (n=2) about 7.4. $E_0$ determines the ionization energy (13.6 eV) of the ground-state hydrogen atom. $n$ and $m$ are the main quantum numbers of the energy levels of both, inner and outer, shells. For a so called $K_\alpha$ transition, where an electron falls from the L into the K-shell, $n$ is 1 and $m$ is 2. Not all electron transitions are allowed. There are selection rules, which the electrons have to follow (see formula 1.3).

$$\triangle n \geq 1 \qquad \triangle l = \pm 1 \qquad \triangle j = 0, \pm 1 \tag{1.3}$$

A scheme for allowed electron transitions is shown in fig. 1.2.

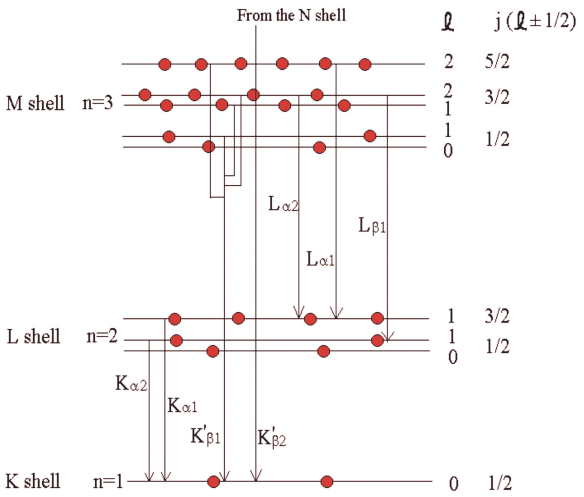


**Figure 1.2:** Generic energy level diagram. (Figure from [Rech et al.])

### 1.1.3 X-ray absorption in material

Electromagnetic-rays interact with matter due to three processes, photoelectric effect, Compton effect and pair production. For typical characteristic X-ray energies (1-30 keV) only the cross-section of photoelectric effect gives an sufficient share to the detection signal.

Unlike the interaction of particles in matter, where the particles like protons lose energy during their way through matter (see subsection 1.1.1), X-rays emit their whole energy to the matter at once. X-rays suffer an intensity loss by interacting with material (see formula 1.4).

$$I(x) = I_0 \cdot e^{-\mu x} \tag{1.4}$$

$I(x)$ is the X-ray intensity after interacting with material during the way $x$, while $I_0$ determines the initial intensity. $\mu$ denotes the linear X-ray absorption coefficient, which depends on the material and the X-ray energy.

## 1.2 GEM - Gas Electron Multiplier

GEM detectors will be used in the next generation of hadron physics with the studying of rare processes with drastically improved sensitivity in mind. For these experiments a detector for charged particles, which has excellent tracking capabilities, will be needed. Such a detector covers large detection areas with flexible geometry and with an extremely low material budget inside of the active area.

The demands made on this detectors are:

- active areas of the order of $m^2$
- spatial resolution of several hundred $\mu m$
- time resolution of a few $ns$
- low material budget inside the active area in order not to spoil the energy and mass resolution of the apparatus
- rate capability of several $10^3 counts/s/mm^2$

### 1.2.1 GEM technology

The Gas Electron Multiplier (GEM) technology bases on a typically 50 $\mu$m thin polyimide foil with a typically 5 $\mu$m thick copper cladding on both sides. A large number of microholes (typically diameter 70 $\mu$m) has been chemically etched into this foil using photolithographic techniques (see fig. 1.3).

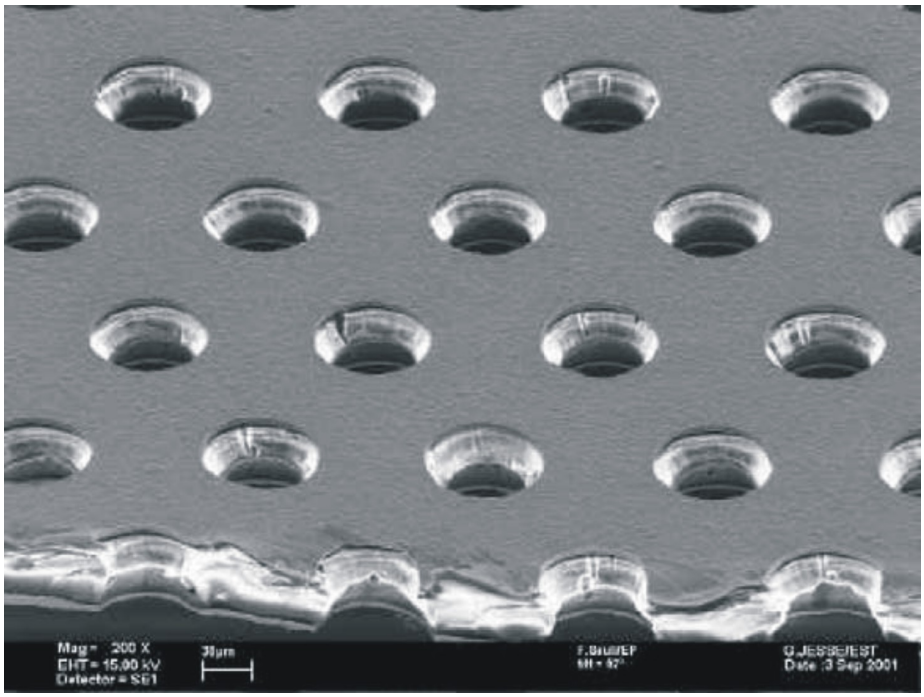


**Figure 1.3:** Electron microscope view of a GEM foil ([Altunbas et al., 2002])

Due to the etching procedure the microholes have a double-conical shape (see fig. 1.4) with a diameter of at least 50 $\mu$m at the waist of the hole.

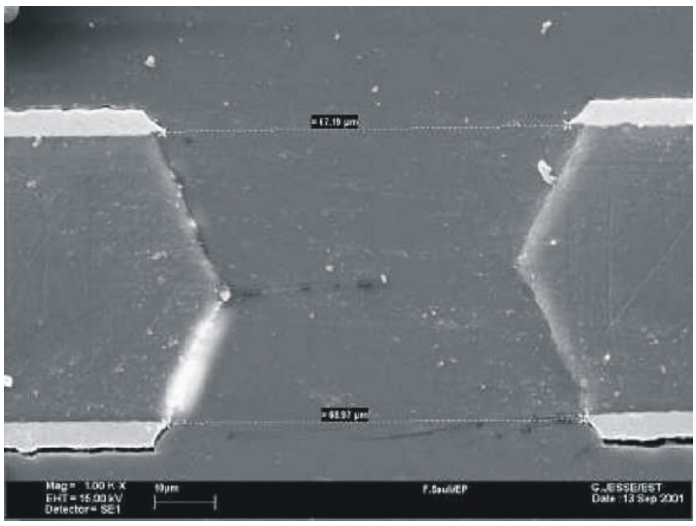

**Figure 1.4:** Electron microscope view of a cross-section through one microhole of a GEM foil ([Altunbas et al., 2002])

A with a voltage difference of several hundred volts can be applied on the two copper sides of the foil. Due to the small size of the holes an electric field of several tens of kV/cm become available inside of each hole. Therefore each hole acts as an multiplication channel for electrons and as an trap for positive charged ions (see fig. 1.5).

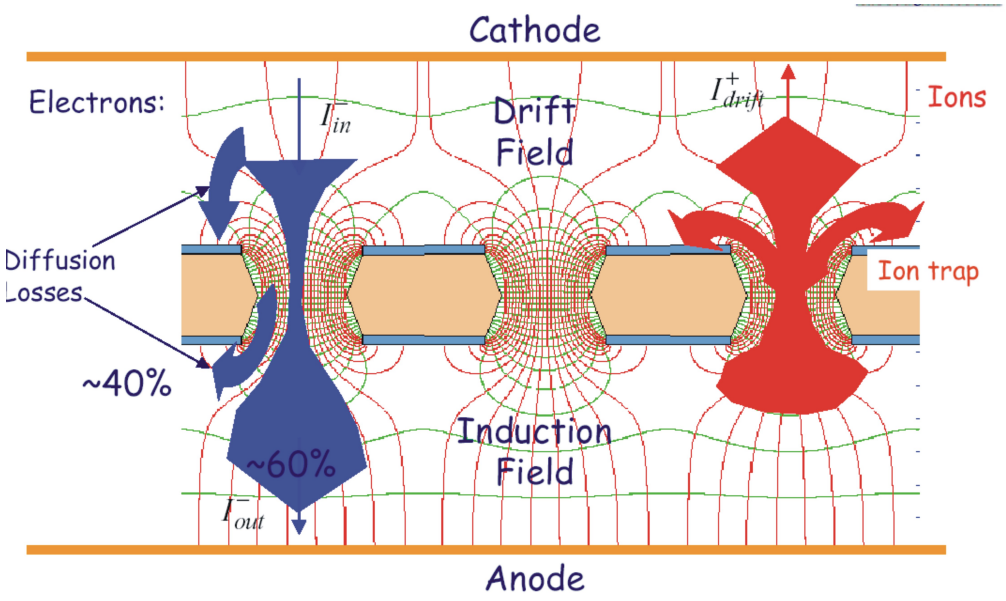


**Figure 1.5:** Electrical fields of a single GEM detector ([Murtas, 2002])

This GEM foil can be mounted inside of a gas detector between the cathode and anode. Such a single GEM detector can reach a multiplication factor of several hundred. Higher gains up to $10^4$-$10^5$ can be achieved by mounting several GEM foils inside of a detector. For this work the reviewed GEM detector had three cascaded GEM foils with a size of $50\,\mathrm{x}\,50\,mm^2$.

A fast signal will be induced on the readout anode from the GEM foil by the emerged electron cloud. The readout anode can be patterned in an almost arbitrary way. Photolithographic techniques are also used here to realize highly granular, thin and flexible structures. The order of the granular structure determine the spatial-resolution of the GEM detector.

# 2 GEM detector

## 2.1 Detector housing

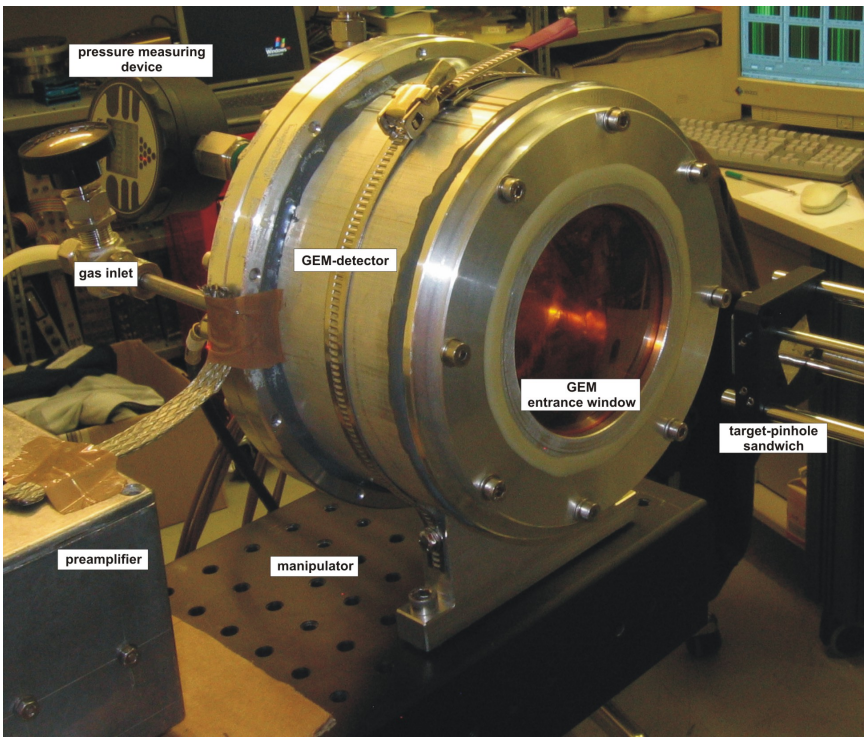


**Figure 2.1:** GEM detector in the measurement assembly

The housing of this GEM detector test equipment is made of aluminum. The weight of the the whole detector with inner life is around 2 kg. The detectors housing is around 150 mm in diameter at its most expanded point and 93 mm thick (see fig. 2.1). The detectors entrance window is made of a 75 $\mu$m thick kapton foil, which is 80 mm in diameter. The gas in- and outlet of the detector are on the back side of the aluminum housing (see fig. 2.2). Inside of the housing the gas is guided to the GEM-foils with four flexible tubes (see fig. 2.4). The gas outlet was connected to a pressure gauge (accuracy of measurement: 1 mbar) whereby the observation of the gas pressure close to the GEM foils was possible (see fig. 2.1). To ensure that no air can get into the detector housing a check valve was also mounted in the gas outlet.

Therefore the gas pressure during the measurements was $1015 \pm 15$ mbar, which was a bit above the atmospheric pressure $970 \pm 20$ mbar of the VERA labor. The final measurements were performed with a $Ar/CH_4$ (90/10%) gas mixture.

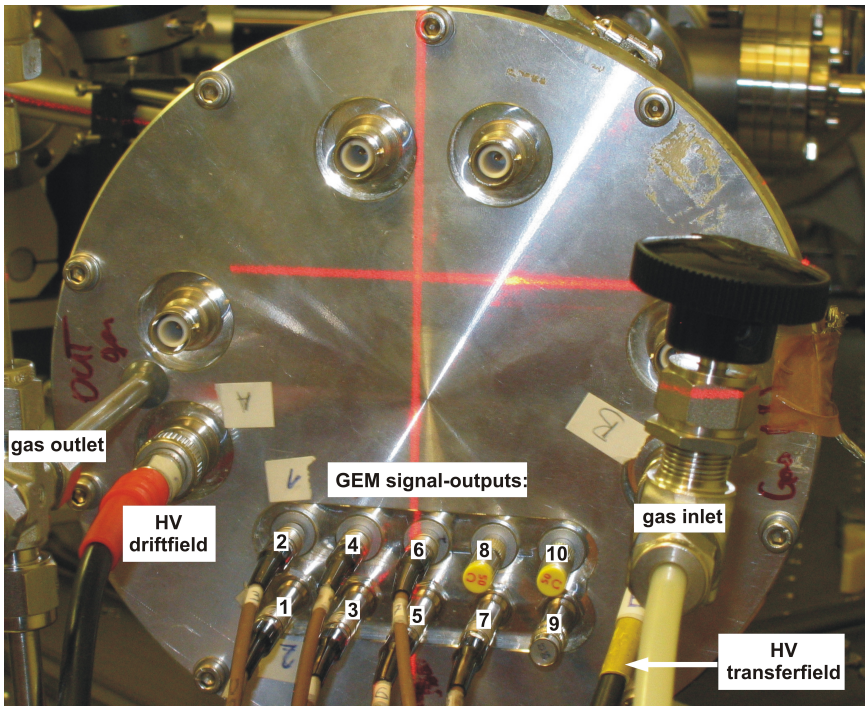


**Figure 2.2:** Back view of the assembled GEM detector

Six high voltage feed-throughs are also mounted on the back side plate of the detector housing. During the measurements only two high voltages were connected on the bottom side of the cathode foil and on the bottom side of the last GEM foil.

For the signal readout ten LEMO connections, one for each readout stripe, are installed on the detectors back side plate (see fig. 2.2). But the signal processing assembly could only work with eight channels at the same time (see fig. 2.7). Therefore only maximum eight stripes were connected to the signal processing assembly at the same time. The remaining LEMO connections were shorted with $50\,\Omega$ resistors to avoid additional signal noise sources.

## 2.2 Inner life of the GEM detector

The inner life of the GEM detector test equipment consist of one cathode foil, three GEM foils and one readout plate with ten separated readout stripes. The cathode foil is a $5\,\mu$m thick aluminum coated mylar foil. A high voltage of -2648 V was connected on the bottom side of this foil. The GEM foils used for this detector are made up of $50\,\mu$m kapton with $5\,\mu$m copper coating on both sides. The holes are biconical

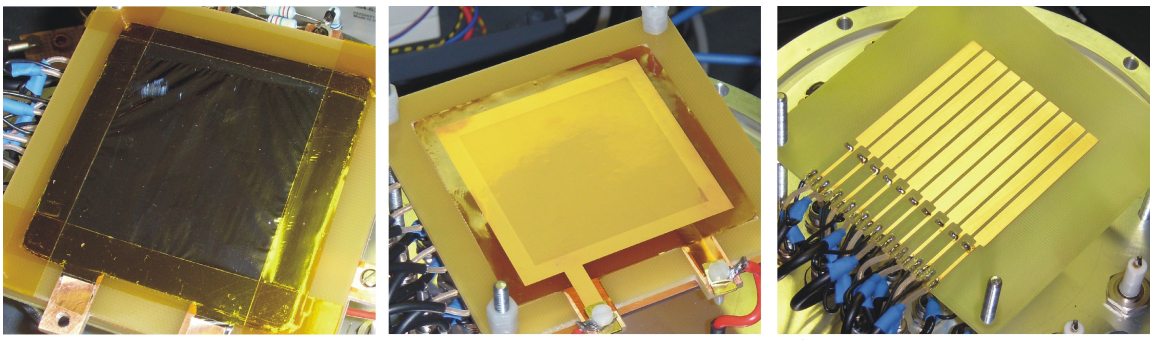


**Figure 2.3:** Inner life of the GEM detector: a)Cathode foil; b)One of three GEM foils; c)Plate with 10 readout-stripes

with a diameter of 70 $\mu$m at the edges and 50 $\mu$m at the waist. The distance between two holes is 140 $\mu$m from center to center. Each foil has a size of $50\,\mathrm{x}\,50\,mm^2$. The mylar foil and the three GEM foils are glued on a frame, which were made of G10 Epoxy fiberglass cloth laminate. On the bottom side of the third GEM foil was a high voltage of -736 V connected.

The readout plate consist of ten copper stripes, which were also glued on a G10 Epoxy fiberglass cloth laminate frame. The stripes are 50 mm long and 4 mm broad. The space between two stripes is 1 mm (see fig. 2.3). The readout stripes were set on ground potential.

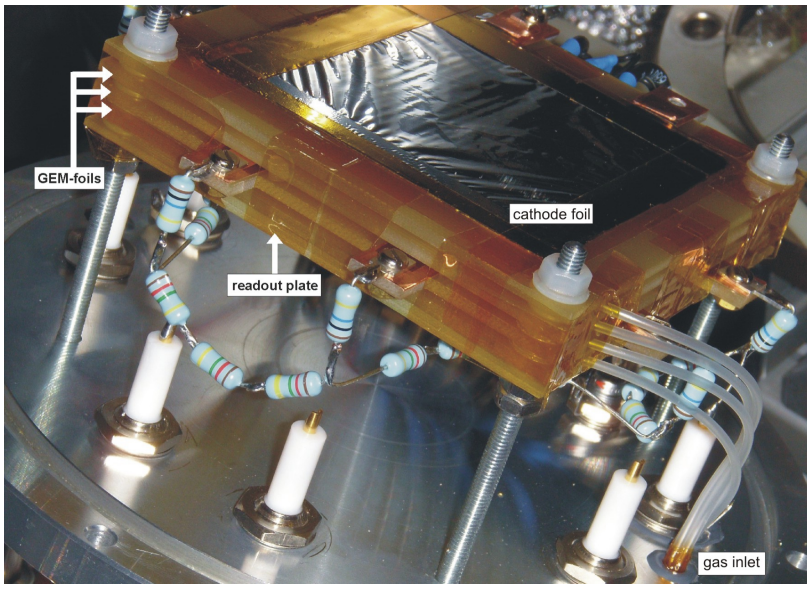


**Figure 2.4:** Inner life of the GEM detector as it was composed in the final measurements

Figure 2.4 shows the layout of the GEM detector. The cathode foil is attached on

the top of of this "foil-sandwich". The readout plate is attached on the bottom side. The three GEM foils are implemented between cathode foil and readout plate in equal distances. The distances between the foils are shown in fig. 2.6. The distance between the detector entrance window and the cathode foil is also shown in fig. 2.6. The gas is guided from the gas inlet to the GEM foils by four flexible tubes, as shown in figure 2.4. This ensures that always "fresh" gas flows around the GEM foils..

A resistor chain is soldered between the bottom side of the cathode foil, where a high voltage of -2648 V was connected, and the bottom side of the third GEM foil, which was connected to -736 V. All copper layers of the GEM foils are connected to this resistor chain (see fig. 2.4). Therefore a voltage difference around 320 V between the single layers is established. A scheme of the voltages supplied to the GEM foils is shown in figure 2.5.

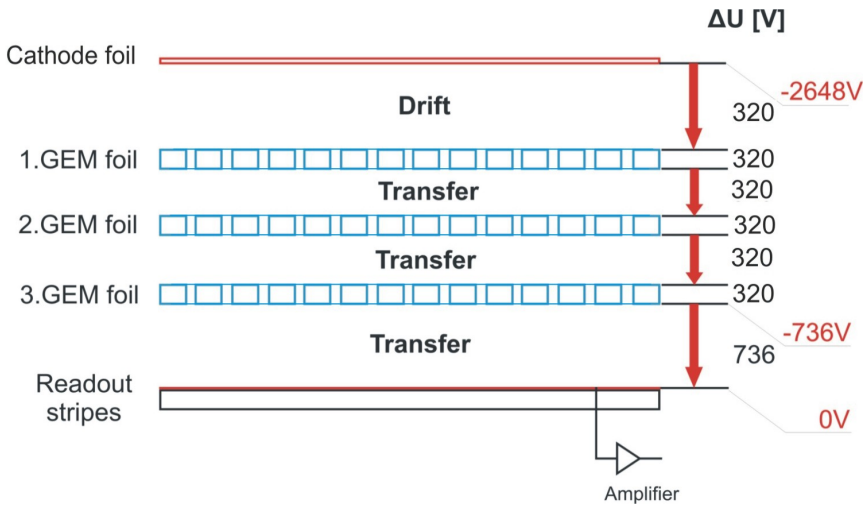


**Figure 2.5:** This figure shows the voltage differences between the single layers inside the GEM detector.

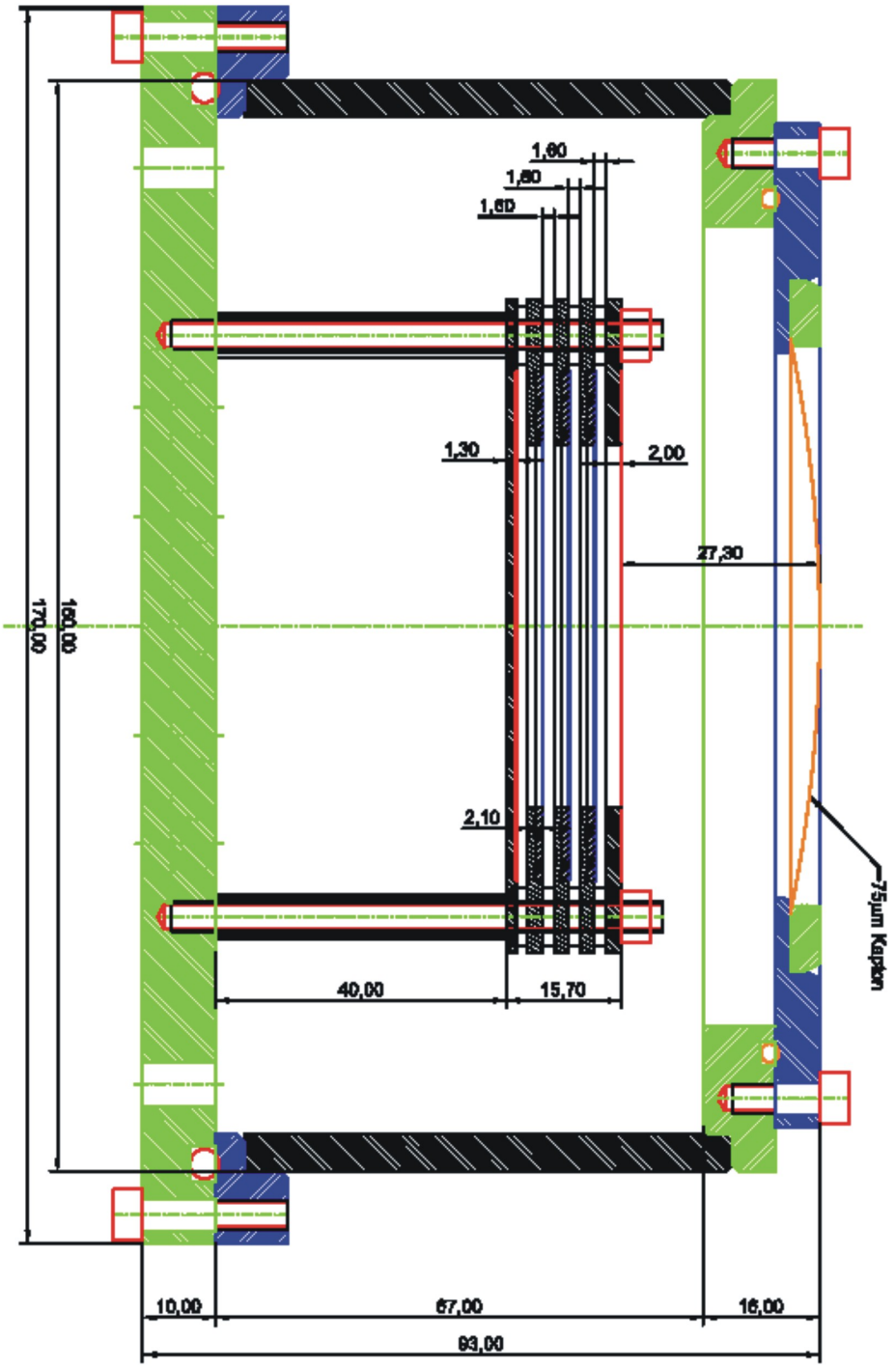


**Figure 2.6:** Detailed geometry of the GEM detector

## 2.3 Signal processing assembly

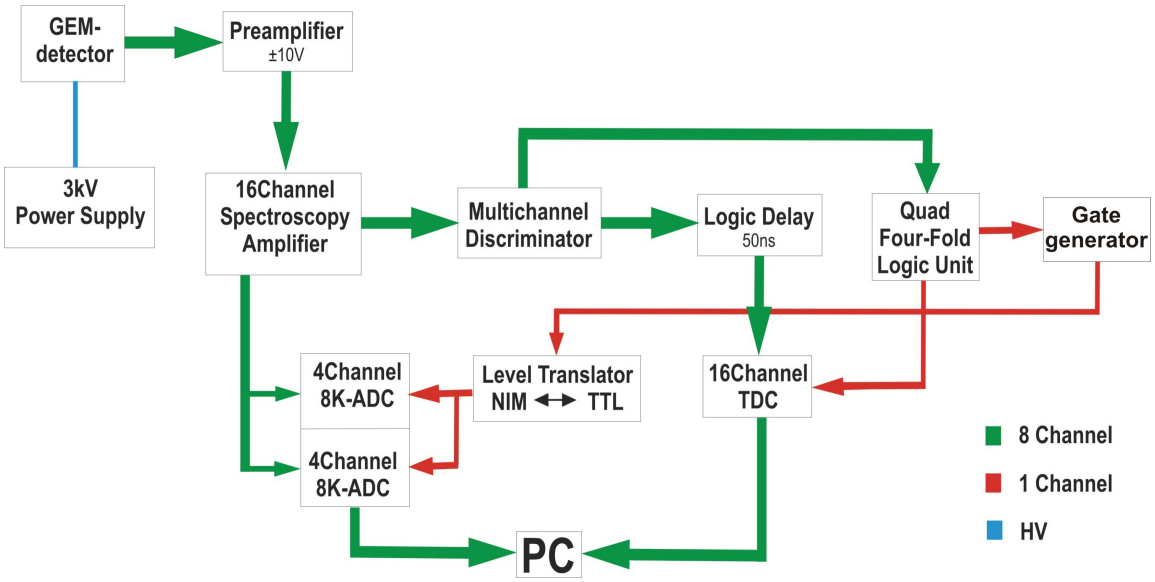


**Figure 2.7:** Scheme of the GEM detector signal processing assembly

The preamplifier, which was used for this signal processing assembly, was self made by the Stefan-Meyer-Institute in Vienna. This preamplifier has ten LEMO connectors for incoming detector signal, which were arranged in two layers to each five LEMO connectors. The output connectors were arranged on both sides of the preamplifier. Two power supplies provided the preamplifier with a range of $+/-10$ V. During the measurements the preamplifier was also mounted on the manipulator close to the GEM detector (see fig. 2.1). The main amplifier was a CAEN 16 Channel Spectroscopy Amplifier Model 568B (16 Channel Spectroscopy Amplifier in fig. 2.7) with two outputs for each channel. One output array (positive signal) was connected to two ORTEC AD413A Quad 8K ADC's (4 Channel 8K-ADC in fig. 2.7).

The second output array (negative signal with fast shaping time) was connected to a PS (Phillips Scientific) Model 710 Octal Discriminator and a PS Model 730 5 Channel Tri-Mode Discriminator (summarized in Multichannel Discriminator in fig. 2.7), which went on in a signal timing processing assembly. With this two discriminators the threshold level could be adjusted manually for each single channel. The second function of the discriminators, besides the threshold level adjustment, were the creation of a time signal of the incoming GEM detector signal for the timing signal processing assembly. The time signal went into a PS Model 756 Quad Four-Fold Logic Unit (Quad Four-Fold Logic Unit in fig. 2.7). This unit combined all eight separated input channels to one common output channel, that means the logic unit creates a output signal, if one of the eight input channels got hit. This common time signal was arrayed to a Technoland corp. 8-ch Gate and Delay Generator,

N-TIM 205 (Gate Generator in fig. 2.7). This generator created a so called "Gate" signal for the two ADC's. The two ADC's only registered signals which were inside of this "Gate". Noise signals did not create a "Gate" and therefore they were not recorded. But there was the problem of the common "Gate" signal for all eight channels. The "Gate" opened all eight ADC channels although only one channel counted a real signal. This means that all other channels counted noise signals at the same time.

For this measurements, the signals from the GEM detector were not only tested for their signal height, but also for their signal timing. The signal timing could be assigned by according to the time of the generated signals. Therefore it was necessary to measure the signals both with the ADC and TDC. The signal timing was measured with a Phillips 7186 16 Channel TDC (16 Channel TDC in fig. 2.7). The signal timing could be analyzed for each channel separately with the TDC data. The TDC got the common start timing signal from the PS Model 756 Quad Four-Fold Logic Unit for all eight channels. The discriminators got a second output to a PS Logic Delay LD 103-A (Logic Delay in fig. 2.7), beside the first one to the PS Model 756 Quad Four-Fold Logic Unit. This logic delay unit creates a time delay of the original time signal of each single channel from the discriminators. The time delay was set to 50 ns so that the individual time signal arrived for sure after the start time signal from the PS Model 756 Quad Four-Fold Logic Unit. In case of a real signal, the TDC records a constant value determined by the delay time, because of a fixed time difference between the common start timing and the signal timing. Thus, analyzing the ADC data having the constant value on the TDC data, the real signal events are properly selected, and the noise signal events are rejected.

The ADC and TDC digital data were sent to a PC with the CAMAC system. There the ADC- and TDC-data were recorded by a special program, based on LABView software and developed by Tomoichi Ishiwatari from the SMI (Stefan Meyer Institute) Vienna.

# 3 Experimental setup

## 3.1 The VERA accelerator

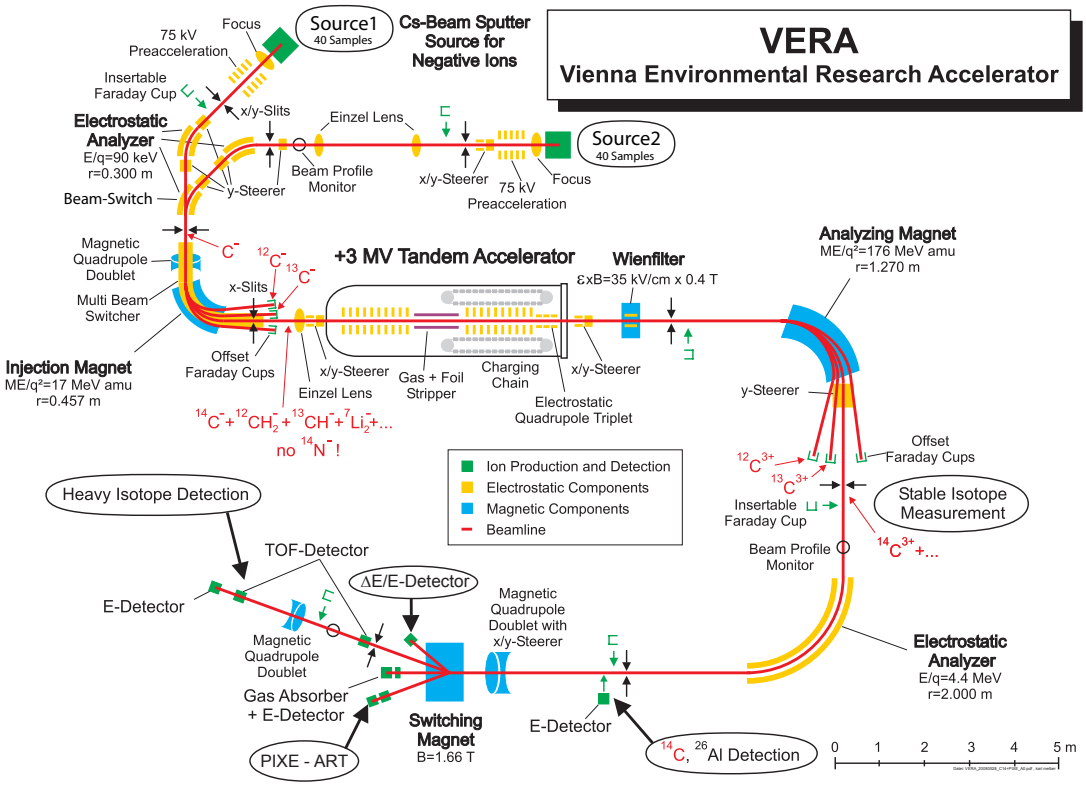


**Figure 3.1:** VERA scheme 2008

VERA (Vienna Environmental Research Accelerator) is a AMS (Accelerator Mass Spectrometry) facility with a 3MV pelletron tandem accelerator built by NEC (National Electrostatics Corporation, Wisconsin, USA)[Kutschera et al., 1997], [Priller et al., 1997]. Since the beginning of the operation in the year 1996 VERA had 3 major upgrades, apart from many little modifications. Figure 3.1 shows a sketch of the actual VERA facility. In 2001 VERA was upgraded with a large electrostatic analyzer, extending its measurement capability range to almost "all" isotopes [Steier et al., 2004], [Priller et al., 2002]. Apart from the main measurement capabilities

of VERA, a separate beam line for performing material analysis (Proton Induced X-Ray Emission, short PIXE) with an external proton beam was installed [Milota et al., 2008]. During the last years a second cesium beam sputter source was designed and integrated in the existing facility in the beginning of this year. The setup for material analysis at VERA has been improved [Reichhart, 2008] and enhanced with other analysis methods like RBS and PIGE [Eder, 2008] during the last year.

Accelerator Mass Spectrometry (AMS) is a very sensitive technique to measure long-lived radioisotopes in an sample material [Kutschera, 1990]. The main principle is the separation of isotopes due to the deflection and acceleration of charged ions with electric and magnetic fields.

The two MCSNICS (Multi Cathode Source of Negative Ions by Cesium Sputtering) of VERA produce negatively charged ions. Both sources are equipped with a cathode wheel, which can hold 40 sample cathodes. For PIXE purposes the cathodes for the old cesium sputter source (Source 1 in fig. 3.1) are $TiH_2$ and for the new source (Source 2 in fig. 3.1) a mixture 1:2 of $HfH_2$ and $Ag$ - powder. The negative charged hydrogen ions are preaccelerated to an energy of 70 keV due to the voltages on the source (see formula 3.1).

$$E = q \cdot U_{Ex} \tag{3.1}$$

with

*E...kinetic energy of the ions*
*q...charge of the ions*
*$U_{Ex}$...extraction Voltage*

The first analyzing element is the 45° electrostatic analyzer (ESA) with a radius of 0.300 m and a maximum $E/q$ of 90 keV (see fig. 3.1). The ESA selects the ions according to their energy (see formula 3.2).

$$\epsilon \cdot r_{ESA} = \frac{2E}{q} \tag{3.2}$$

with

*$\epsilon$...electric field of the ESA*
*$r_{ESA}$...radius of the ESA (0.300 m)*
*E...kinetic energy of the ions*
*q...charge of the ions*

After the electrostatic analyzer the ion beam will be deflected with a 90° analyzing magnet, called injection magnet in fig. 3.1. The analyzing magnet selects ions according to their momentum. Due to the combination with the ESA it is selective according to the mass of the ions (see formula 3.3).

$$B \cdot r_{BM} = \frac{p}{qe} \qquad (3.3)$$
$$p = \sqrt{2mE}$$

with

*B...magnetic field of the injection magnet (max. 1.25 T)*
*$r_{BM}$...radius of the injection magnet (0.457 m)*
*E...kinetic energy of the ions*
*m...mass of the ions*
*q...charge of the ions*

The 3MV Pelletron Tandem Accelerator is the heart of VERA. Both ends of the accelerator are on ground potential, the middle of the tank is on 1.5 MV positive high voltage. Negatively charged ions are accelerated to 1.5 MeV by the first cascade of ring electrodes. In the middle of the accelerator the ions collide with a stripper gas, which removes the electrons from the hydrogen ions. This ensures the acceleration of the now positively charged ions ($H^+$) for a second time. At the exit of the accelerator the hydrogen ions have an energy of 3 MeV, which is the usual energy for PIXE measurements.

Another analyzing magnet ($B_{max} = 1.53$ T, r = 1.27 m) and ESA ($\epsilon_{max} = 55$ kV/cm, $r_{ESA} = 2.000$ m) combination on the high energy side of the accelerator leads the $H^+$ beam into the switcher magnet (see fig. 3.1). This magnet has the capability to switch between several different beam lines for different analyzing purposes. For our purpose we used the -20° , the PIXE-ART, beam line (see fig. 3.1).

Apart from the already described main components of VERA, there are multiple beam focusing components. Plate capacitors, called Steerers, permit a better positioning of the beam within the beam line. Magnetic Quadrupole doublets give the possibility to focus the beam.

## 3.2 The PIXE setup

At the end of the PIXE-ART beam line a nozzle is positioned (see fig. 3.2). This nozzle is a 10 cm long stainless steel tube with a diameter of 6 mm and a pure carbon collimator with a 150 $\mu$m hole within. On the crossover from vacuum (in the order of $10^{-4}$ mbar) to atmospheric pressure a 100 nm thick $Si_3N_4$ exit window is glued on the carbon collimator [Milota et al., 2008].

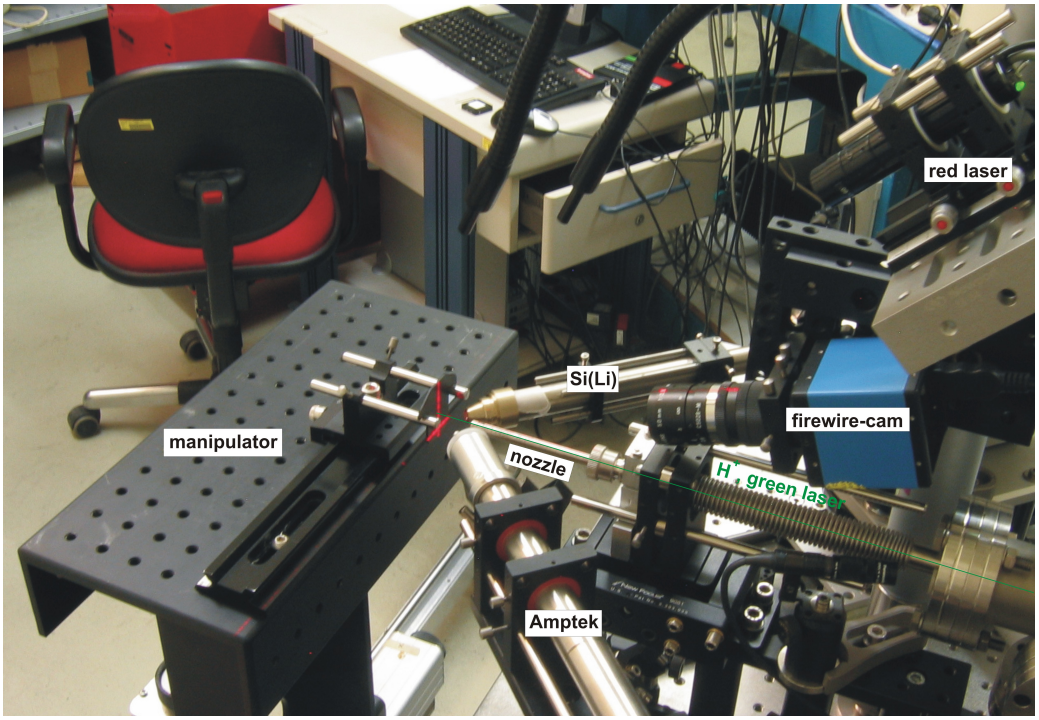


**Figure 3.2:** PIXE-ART beam line at VERA

This nozzle can be changed if the exit window is leaky. For a reproducible change of the nozzle a red cross laser is mounted on the wall opposite to the PIXE-ART beam line. An exact alignment of the nozzle is given, if the middle of the nozzle hole fits with the crosspoint of this laser (see fig. 3.3).

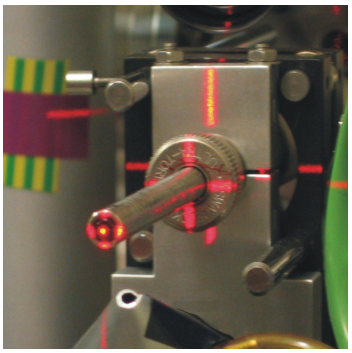

**Figure 3.3:** Nozzle positioning via cross laser

One of the big tasks of material analysis with external proton beam is the reproducibility of the target position. Therefore a green laser is attached at the switcher magnet chamber. The beam of the green laser is going collinear with the proton beam through the PIXE-ART beam line and creates a spot on the external target.

In addition a red laser (cross shaped) is positioned at an 45° angle above the beam line (see fig. 3.2). The two lasers cross 1 cm in front of the nozzle. The targets can be attached on a three axis computer controlled positioning table. The smallest stepsize, which the table can be moved, is 50 $\mu$m with an accuracy of $\pm 10\,\mu$m. With this "manipulator" the targets can be reproducibly positioned at the reference point, which is defined by the crosspoint of the lasers. For a better observation a fire-wire camera, which is focused on the crosspoint, is installed between beam line and red laser (see fig. 3.2).

## 3.3 Measurement assembly

The main goal of this work was the examination of the location-dependence of the efficiency and signal amplification across the detection area of the GEM detector.

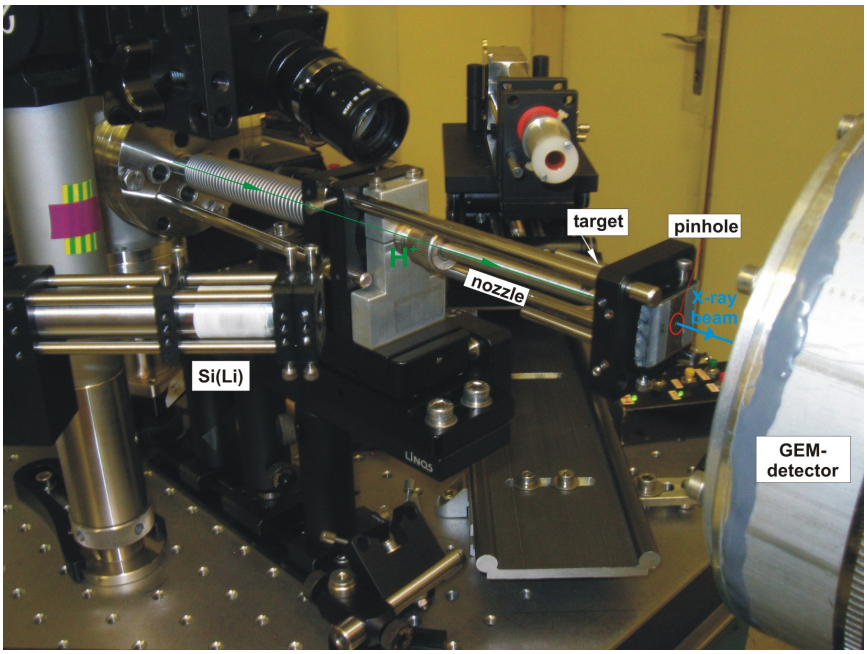


**Figure 3.4:** Measurement assembly of the final GEM-tests

As PIXE - target for characteristic X-ray production a stainless-steel foil was positioned at the lasers crosspoint. The foil was a stainless-steel precision gauge tape ($20 \pm 2\,\mu$m, Material-No.: 1.4301) from the "Hasberg-Schneider GmbH" company.

The chemical composition of the precision gauge tape:

| **Element** | [%] |
|---|---|
| Fe | 67 - 72 |
| Cr | 17 - 20 |
| Ni | 8.5 - 10 |
| Mn | 2 |
| Si | 1 |
| C | 0.07 |
| P | $< 0.045$ |
| S | $< 0.03$ |

**Table 3.1:** Chemical composition of the target foil ([Hasberg-Schneider, 2000])

Behind the target foil a pinhole was attached. This pinhole was a 1 mm thick stainless-steel pad, where a hole with a diameter of 500 $\mu$m was drilled (see fig. 3.5). At the final measurements the distance between target and pinhole was set at 15 mm (see fig. 3.5). A measurement to determine the most suitable distance between target and pinhole was made before the main measurements were accomplished (see chapter 4).

This setup ensured, that the X-rays produced in the target could only pass through the pinhole. In such a way restricted, it was possible to excite only a small area of the GEM detector (see section 4.1).

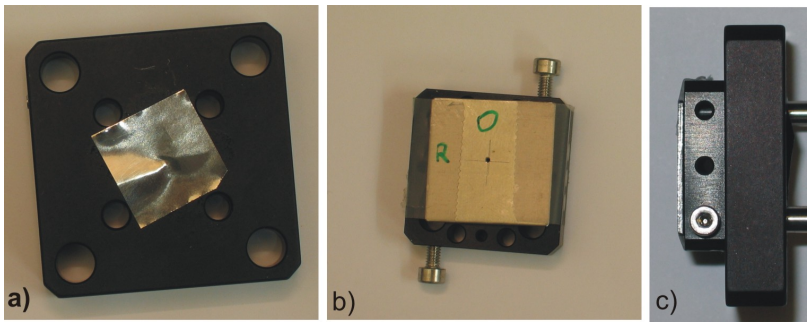


**Figure 3.5:** a)20 $\mu$m Stainless steel foil; b)1 mm thick stainless steel pad with a 500 $\mu$m pinhole; c)Top view of the target-pinhole sandwich as it was used during the measurements. The distance between target and pinhole was 15 mm.

For the GEM detector measurements a second X-ray detector was added to the assembly. This 30 mm$^2$ Si(Li) X-ray detector (e2v) was placed at an angle of 45° relative to the external proton beam (see fig. 3.2, 3.4, 3.6) in a distance of 95 mm to the target foil. The Si(Li) was used as an reference for the data of the GEM detector (see chapter 4.1). Due to the fluctuation of the $H^+$ beam intensity, the X-ray production in the target foil is not constant. Thus a direct comparison of

two GEM measurements is not possible. The Si(Li) detector monitors the same fluctuation, but unlike the GEM detector the intrinsic efficiency of the Si(Li) is constant. The measured events of the GEM detector become independent of the $H^+$ beam fluctuation when normalised to the measured events of the Si(Li).

$$n_{rel}[\%] = 100 \cdot \frac{N_{GEM}}{N_{SiLi}} \tag{3.4}$$

with

$$n_{rel}...relative\ number\ of\ events\ GEM/Si(Li)$$
$$N_{GEM}..number\ of\ events\ of\ GEM$$
$$N_{SiLi}...number\ of\ events\ of\ Si(Li)$$

One of the requirements on the measurements assembly was the movability of the setup. Therefore the GEM detector itself was mounted on the positioning table just in front of the PIXE-ART beam line. Therefore it was possible to move the GEM detector through the X-ray beam spot and reach all points of the whole detection area. The distance of the GEM detector to the pinhole was 45 mm during the final tests. A drawing of the setups configuration is given in fig. 3.6.

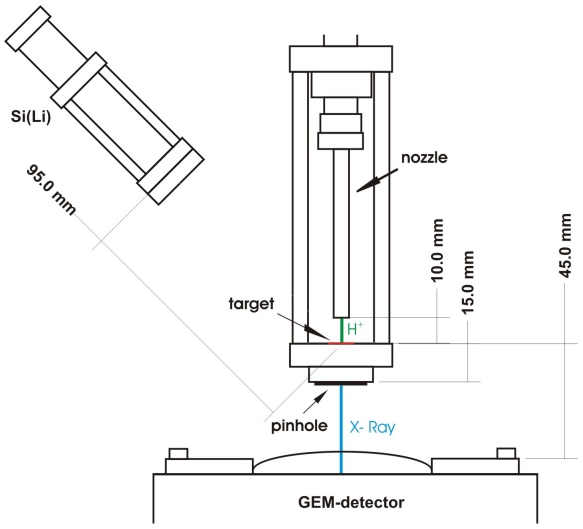


**Figure 3.6:** Drawing of the measurements distances during the final GEM-test

# 4 Measurements and Results

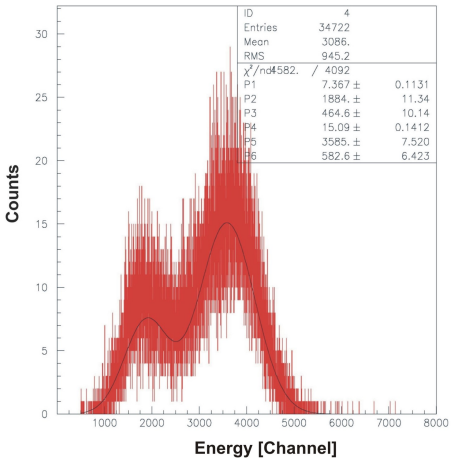


**Figure 4.1:** Energy spectrum of the steel target, measured with the GEM-detector (Stripe 4)

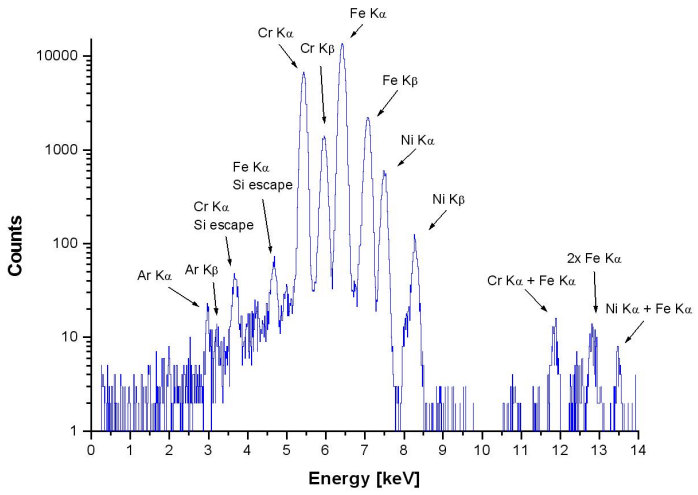


**Figure 4.2:** Energy spectrum of the steel target, measured with the Si(Li) X-ray detector. (Note logarithmic scale!)

Fig. 4.1 and fig. 4.2 show typical X-ray energy spectra of the stainless steel target (see fig. 3.5) recorded with stripe 4 of the GEM-detector and the Si(Li) X-ray detector. The double peak of the GEM-detector is clearly visible. At the Si(Li) energy spectrum the $K\alpha$ and $K\beta$ X-ray peaks of Fe, Cr and Ni are well viewable.

| **Peak** | **Energy / FWHM[keV]** | **theoretical Energy [keV]** |
|---|---|---|
| Ar-$K\alpha$ | 2.94 / - | 2.96 |
| Ar-$K\beta$ | - | 3.19 |
| Cr-$K\alpha$ | 5.41 / 0.133 | 5.41 |
| Cr-$K\beta$ | 5.93 / 0.154 | 5.95 |
| Fe-$K\alpha$ | 6.40 / 0.143 | 6.40 |
| Fe-$K\beta$ | 7.05 / 0.152 | 7.06 |
| Ni-$K\alpha$ | 7.47 / 0.135 | 7.47 |
| Ni-$K\beta$ | 8.27 / - | 8.26 |

**Table 4.1:** X-ray energies of the with the Si(Li) detected elements. Theoretical values are from [Thompson et al., 2001]

The problem of the GEM-detector double peak arose already at the first test measurements with an $^{55}$Fe X-ray source. The X-ray energies of the $^{55}$Fe source are the $K\alpha$ and $K\beta$ lines of $^{55}$Mn at 5.89 keV and 6.49 keV. The energy resolution of the GEM-detector is to big for a differentiation of the two $^{55}$Mn peaks. Therefore it was a question, what the second smaller peak is. On a second look it is obvious that the second peak has half of the energy of the $^{55}$Mn X-ray peak. One of the possible explanations is, that some signals become split between two neighboring stripes, so that each stripe register a signal with half of the energy.

Therefore a particular test were performed, where only stripe 3 and stripe 4 were connected to the preamplifier during a measurement with an $^{55}$Fe source. As mentioned in section 2.3, it is possible with the signal processing assembly to record the time of each signal. So it was possible to determine which signals hit different stripes at the same time. The results of this test are shown in fig. 4.3.

The upper two graphics are the energy spectra of stripe 3 and stripe 4. At the graphic in the lower left corner of fig. 4.3 the two energy spectra are plotted against each other. Each point is a signal, which was detected at the stripes at the same time. We got the additional information about the detected energy of this signal in each stripe. By comparison with the two energy spectra of stripe 3 and stripe 4 it is obvious, that the center of the "double-signals" is nearly at the same energy than the two lower peaks at the energy spectra. If we add for each point the energies of both stripes, than we get the spectrum, which is shown in the lower right corner of fig. 4.3. The position of the peak mean is nearly equal to the peak mean of the $^{55}$Mn peak of both stripes.

But the low number, which has been marked in red in the two lower graphics in fig. 4.3, of this points indicates, that is only a small contribution to the lower peaks

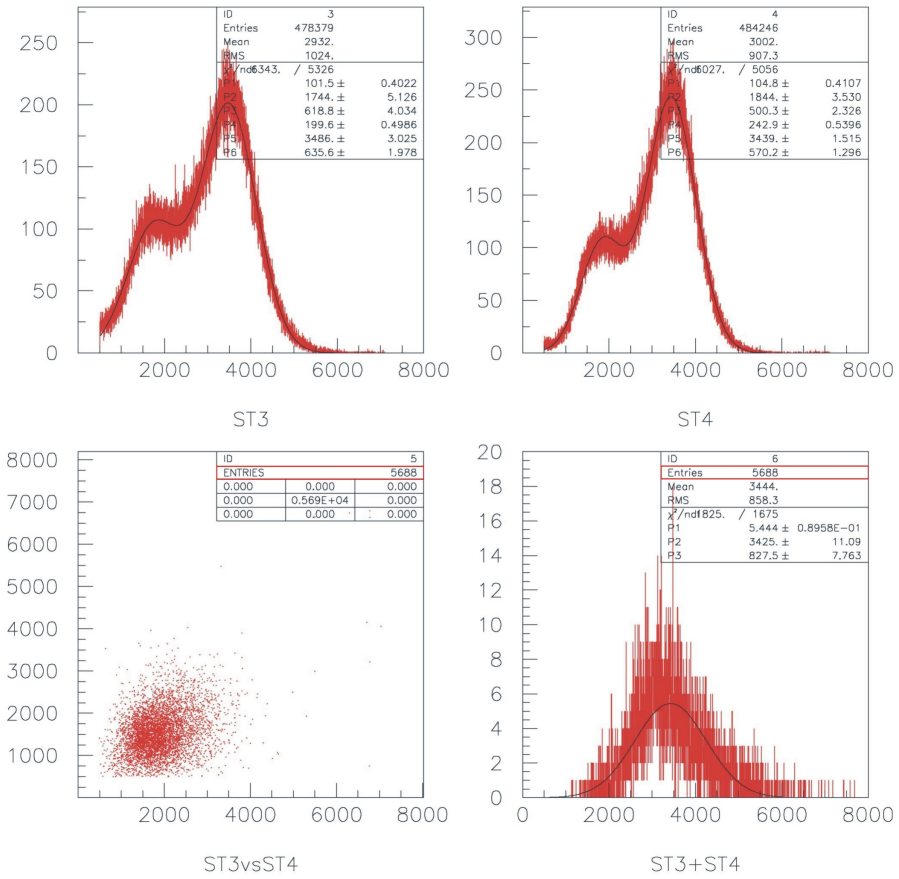


**Figure 4.3:** Test measurement of stripe 3 and stripe 4 of the GEM-detector with $^{55}Fe$

and that the idea of the "split signals" is not the only explanation for this low energy peaks.

The main part of these peaks are Ar-fluorescence signals. Due to excitation of the Ar-atoms of the $Ar/CH_4$ gas inside of the detector by interaction with the Mn X-rays, Ar-$K\alpha$ and Ar-$K\beta$ X-rays with an energy of 2.96 keV and 3.19 keV can be produced. These X-rays are also detected by the GEM-detector.

## 4.1 Pinhole-GEM distance measurements

The intention of this measurements was the determination of the most suitable position of the pinhole between target and GEM-detector (see fig. 4.4). The size of the X-ray beam spot on the cathode foil depends on the position of the pinhole.The distance between target and GEM detector entrance window is set to 45 mm. The number of x-rays, which pass the pinhole and become detectable, decreases with larger distance between target and pinhole (= smaller distance between pinhole and

GEM detector). This causes a smaller number of events in the GEM-detector.

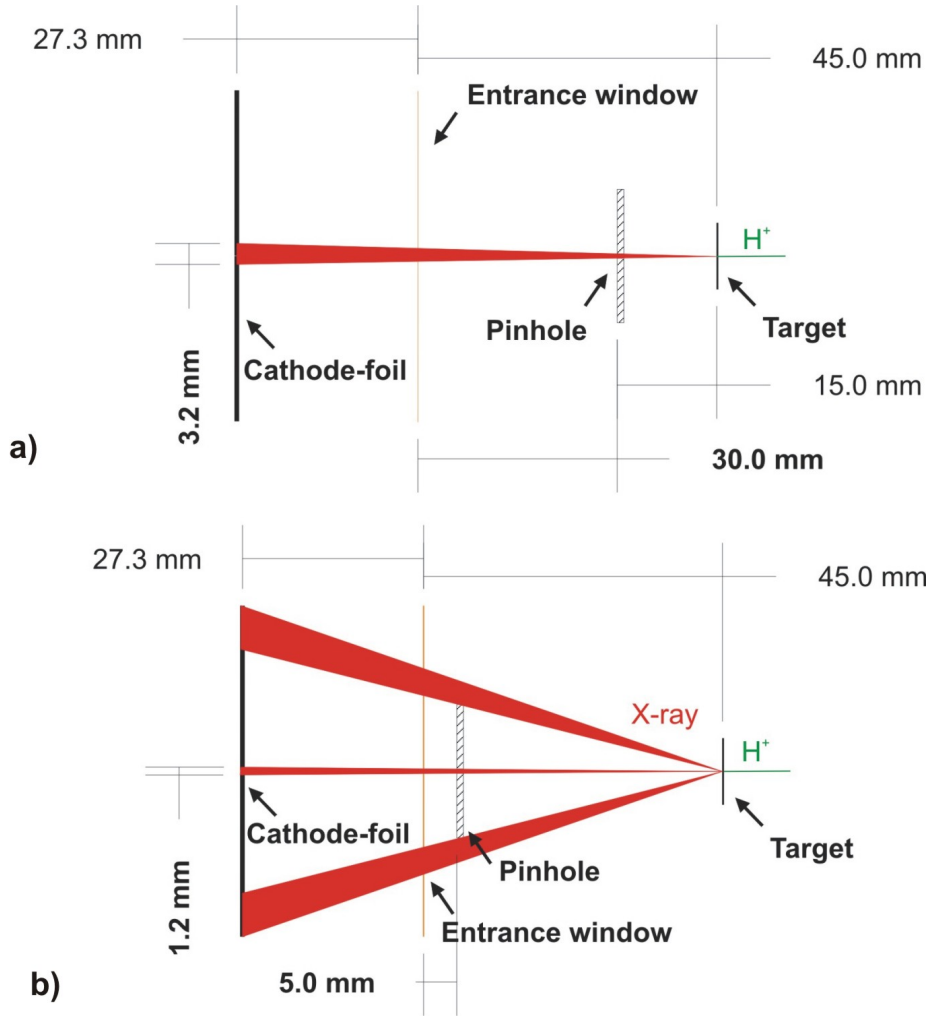


**Figure 4.4:** a)X-ray spot size on the cathode foil of the GEM-detector at a pinhole - GEM detector distance of 30 mm. b)X-ray spot size on the cathode foil of the GEM-detector at a pinhole - GEM detector distance of 5 mm.

Fig. 4.4 shows the size of the X-ray spot at different pinhole positions due to geometrical effects. A decreasing of the distance between pinhole and GEM detector from 30 mm to 5 mm causes a decreasing of the X-ray spot size from 3.2 mm to 1.2 mm.

A small distance between pinhole and GEM detector also has another effect. If the distance between GEM detector and pinhole is small enough, the pinhole pad does not shield the whole detection area of the GEM detector from the X-rays. Thereby some X-rays had not to pass the pinhole to reach the detection area of the GEM detector (see fig. 4.4.b).

The number of detected events in the GEM detector was measured for each pinhole position and compared with the number of events in the Si(Li). At the beginning the pinhole was situated at the closest position to the target at a distance of 30 mm to the GEM detector. Then the distance was decreased in 5 mm steps to an end distance between pinhole and GEM detector of 5 mm. The GEM detector was positioned in such a way during the measurements, that the X-ray beam spot hits the detection area just under the upper edge of stripe 5.

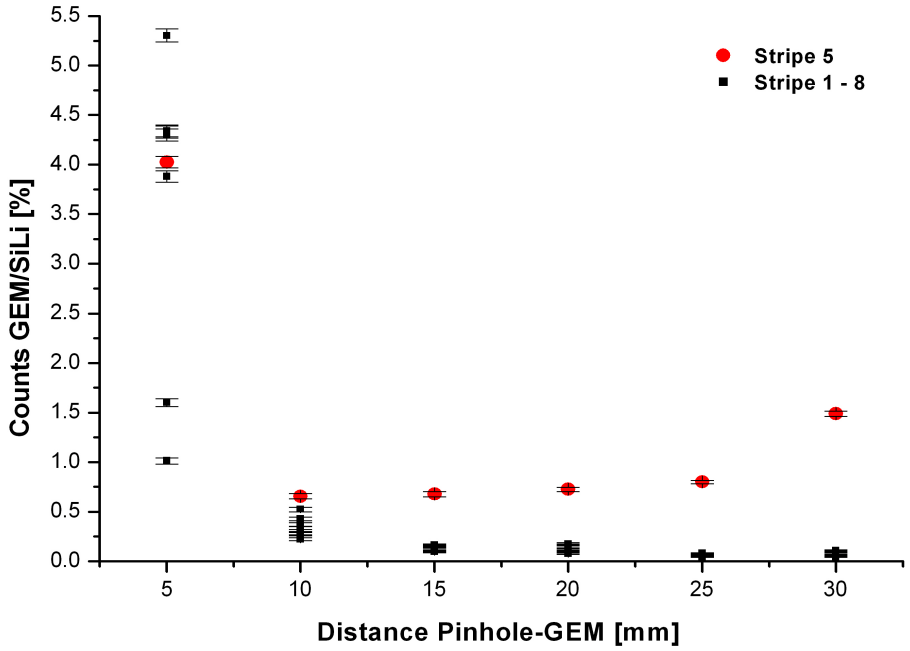


**Figure 4.5:** Number of events in GEM detector compare with number of events in Si(Li) depending on the distance between pinhole and GEM detector

Fig. 4.5 shows the result of these measurements. The number of events in the GEM detector is only around 1.5% compared to the Si(Li) at a distance of 30 mm between pinhole and GEM detector. If the distance decreased to less than 20 mm, the number of events was two times smaller than at a distance of 30 mm. A distance between pinhole and GEM detector of less than 10 mm implicate detectable X-rays in the other stripes. This was recognisable due to the increasing number of events in the other stripes. At a distance of 5 mm between pinhole and GEM detector the number of events in other stripes was three to four times bigger than the number of events in stripe 5 at 30 mm between pinhole and GEM detector. Thus it appeared that the X-rays hit the outer detection area of the GEM detector and therefore the

shielding effect of the pinhole was repealed.

The distance between pinhole and GEM detector was chosen with 30 mm at the final measurements, due to the results of these measurements. The spatial resolution of the GEM detector is mainly given by the width of the readout stripes of 4 mm. Therefore it is needless to restrict the X-ray beam size to a much lesser magnitude.

## 4.2 Final Measurements

The location dependence of the efficiency and the signal amplification across the detection area of the GEM detector was examined at the final measurements. For that purpose several measurement runs were performed across the detection area of the GEM detector. In particular measurement runs were made across all ten stripes and along stripe 3 and along stripe 4. Each measurement run was done twice. The stepsize between the single measurement points of the runs were 1 mm. The measurement time for each point was 300 s.

The error bars for the efficiency-plots in the next sections were calculated via error propagation of the standard deviation of the number of events of the GEM detector and Si(Li).

$$\left(\frac{\sigma_n}{n_{rel}}\right)^2 = \left(\frac{\sigma_{GEM}}{N_{GEM}}\right)^2 + \left(\frac{\sigma_{SiLi}}{N_{SiLi}}\right)^2 \tag{4.1}$$

with

$\frac{\sigma_n}{n_{rel}}$ *...relative uncertainty of* $n_{rel}$ *(see formula 3.4)*

$\frac{\sigma_{GEM}}{N_{GEM}}$ *...relative uncertainty of the GEM detector*

$\frac{\sigma_{SiLi}}{N_{SiLi}}$ *...relative uncertainty of Si(Li)*

The positions of the peak mean of each measurement point were determined by gaussian fits. The plotted error bars of the peak positions are the uncertainties of these gaussian fits.

The x-axis label of the following graphics describes the position of the 3-axis computer controlled manipulator in horizontal or vertical direction, respectively.

### 4.2.1 Scan across all 10 stripes

The following three graphics show the results of the scan across the ten stripes. The maximum of the peaks of all ten stripes is well noticeable. The peak in the right-most position shows the number of events of stripe 1 at the scan. The peak in the left-most position shows the number of events of stripe 10.

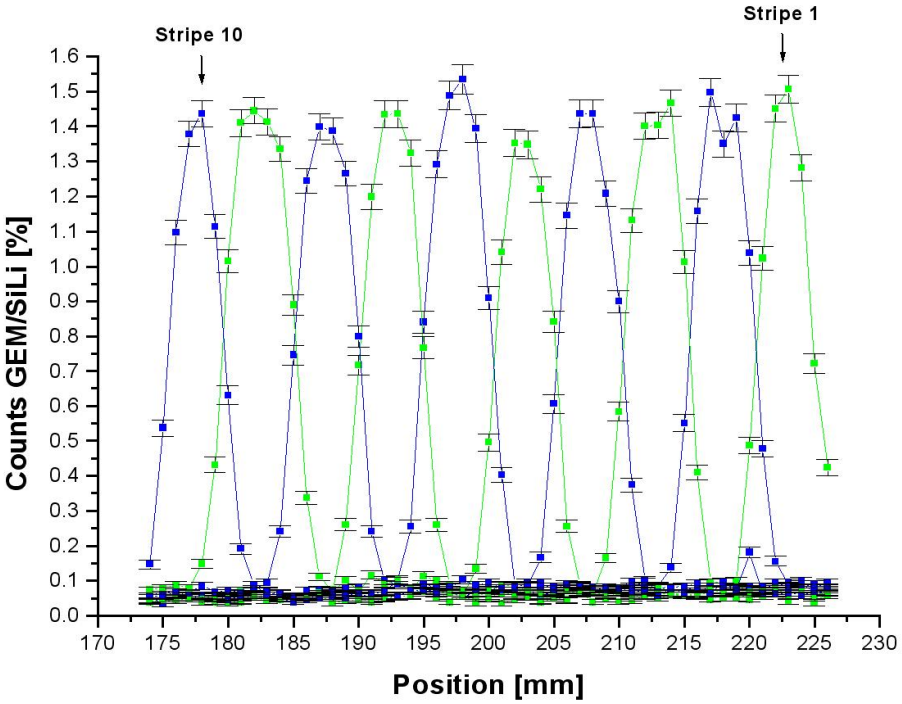


**Figure 4.6:** First efficiency scan across all ten stripes

Fig. 4.6 shows the number of events in the GEM detector relative to the Si(Li) of the first scan across all ten stripes. All peak heights are in the same order. The small variation of the peak height is caused by standard deviation of the single measurements.

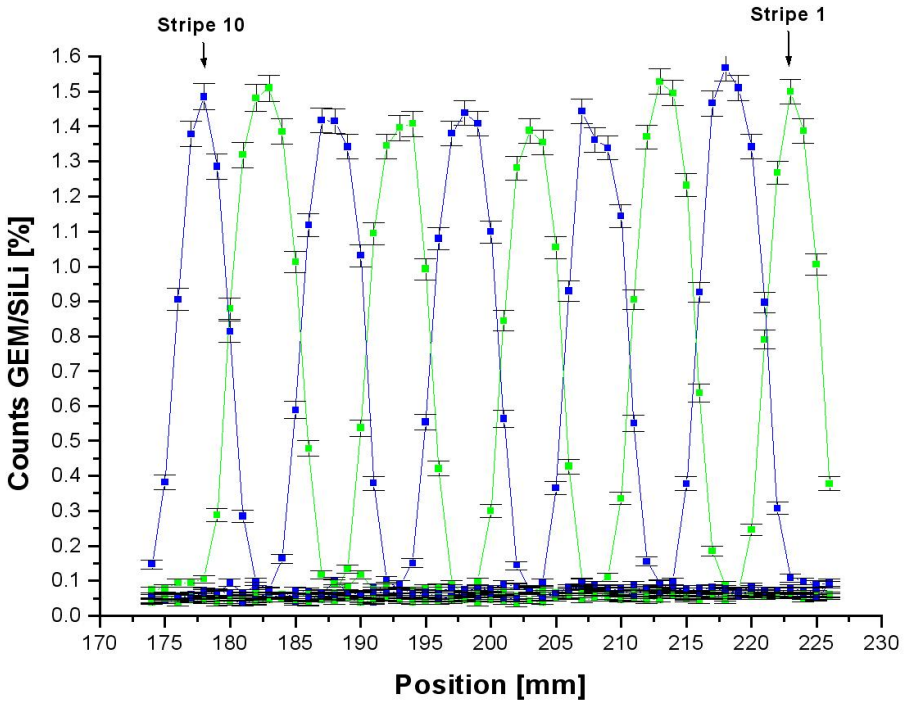


**Figure 4.7:** Second efficiency scan across all ten stripes

Fig. 4.7 shows the number of events in the GEM detector relative to the Si(Li) of the second scan across all ten stripes. Like in the first scan the peak heights of all ten stripes are in the same order.

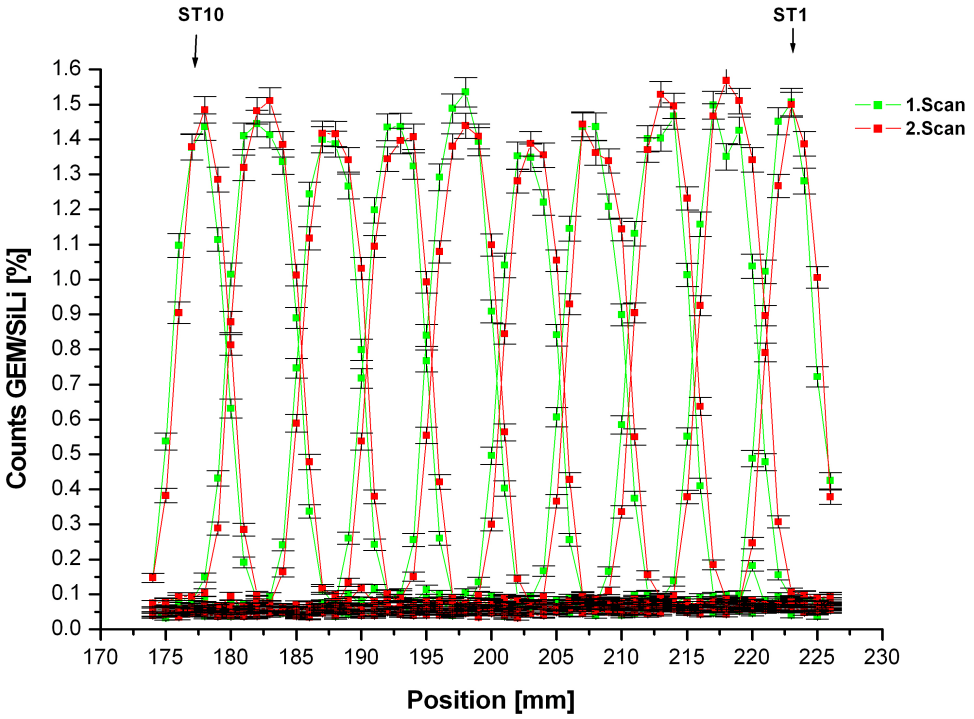


**Figure 4.8:** Both efficiency scans across all ten stripes by comparison

Fig. 4.8 shows both scans across all ten stripes by comparison. The reproducibility of the measurement is clearly shown.

Fig. 4.9 shows the energy spectra of stripe 1 to stripe 8 without pinhole between X-ray target and GEM detector. It is obvious, that the peak heights of each stripe are at different channels. This implies different amplification of the signals for each stripe. These amplification differences could not be eliminated till the final measurements. The gas- and the preamplifier amplification of the signals could not be measured independently. Therefore it was impossible to determine a potential irregular signal amplification between different stripes of the GEM detector.

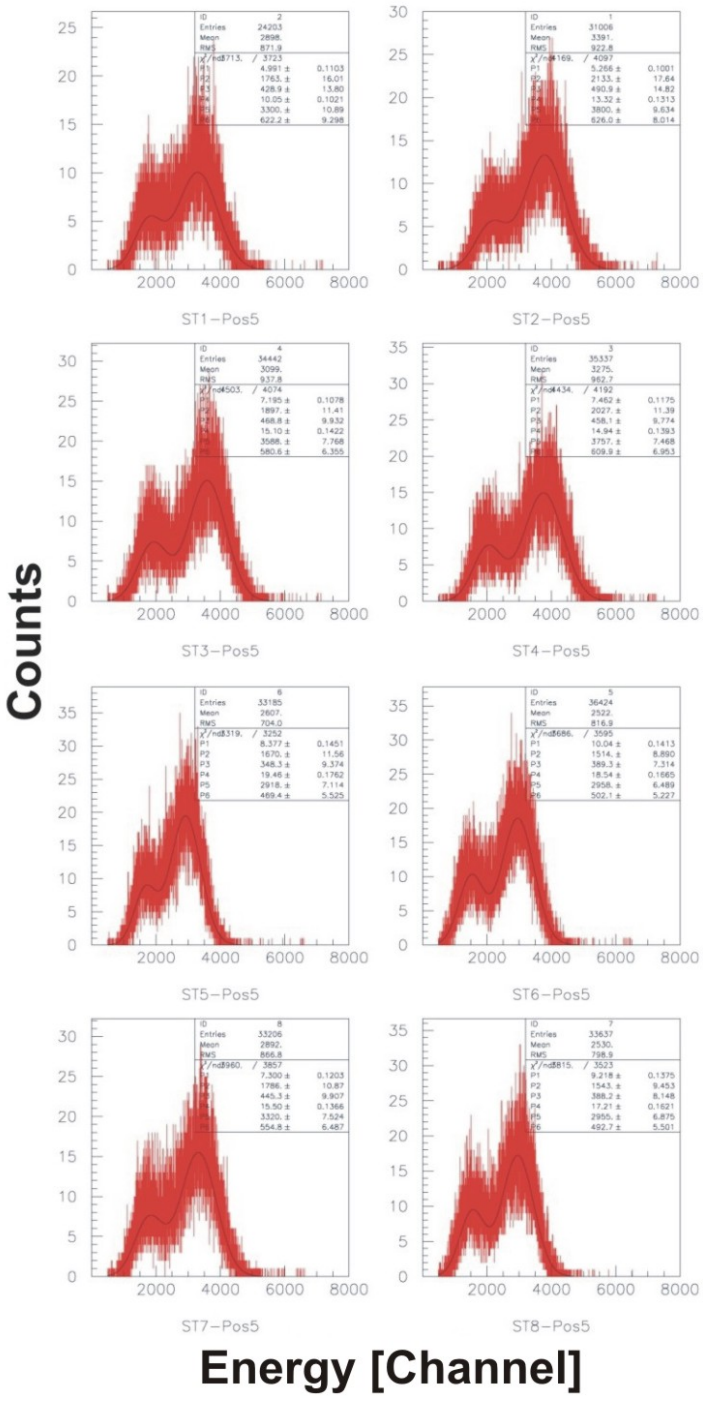


**Figure 4.9:** Energy spectra of stripe 1 to stripe 8

### 4.2.2 Scan along stripe 3

The measurement runs along stripe 3 and stripe 4 are going few mm beyond the edges of the stripes. Because the X-ray spot does not or partially hit the detection area a fast fall of the number of events toward 0 % at the edges of the data point series are noticeable.

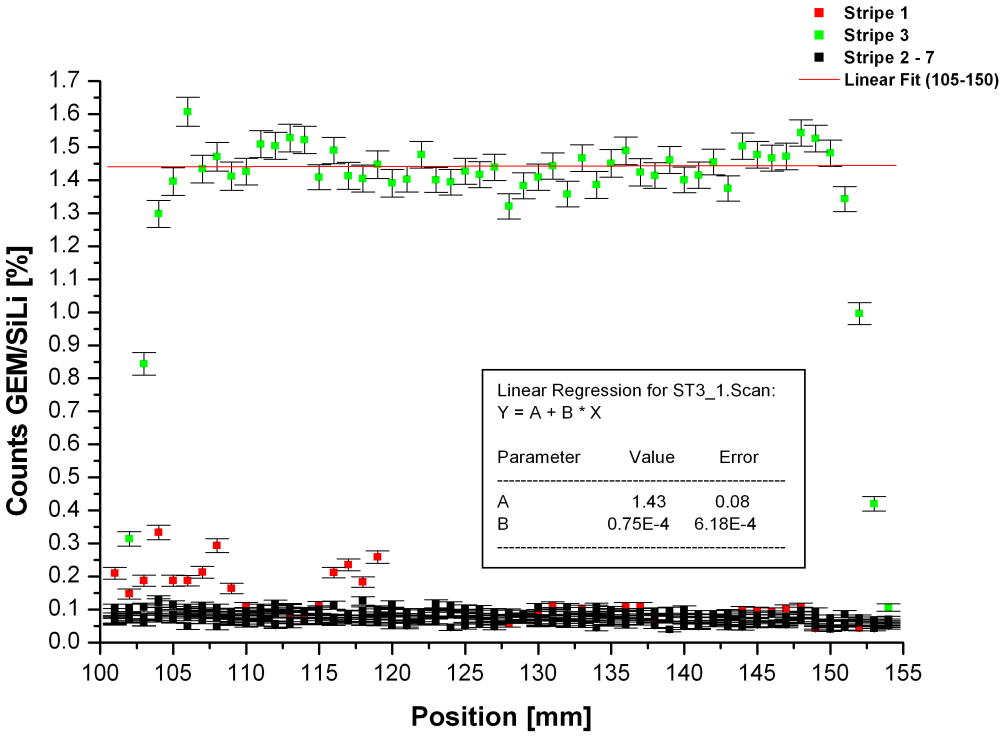


**Figure 4.10:** First efficiency scan along stripe 3

Fig. 4.10 shows the number of events of the GEM detector relative to the Si(Li) of the first measurement run along stripe 3. The linear fit of the data points from vertical manipulator position 105 mm to 150 mm shows an insignificant gradient. This small gradient implies constant efficiency along stripe 3. Conspicuous is the high number of events between 100 mm and 120 mm comparative to the other stripes. This large number of events are noise events, which were created by strong movement of the microphonic preamplifier during the measurements.

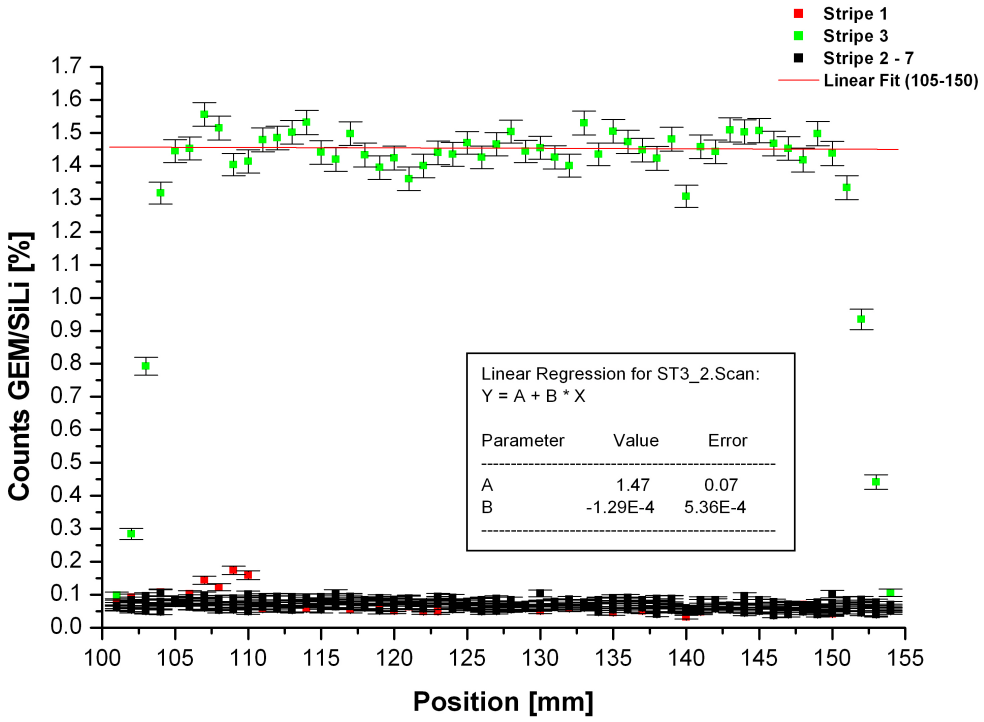


**Figure 4.11:** Second efficiency scan along stripe 3

Fig. 4.11 shows the number of events of the GEM detector relative to the Si(Li) of the second measurement run along stripe 3. Like in the first scan the data points are in the same order. The linear fit shows also constant efficiency

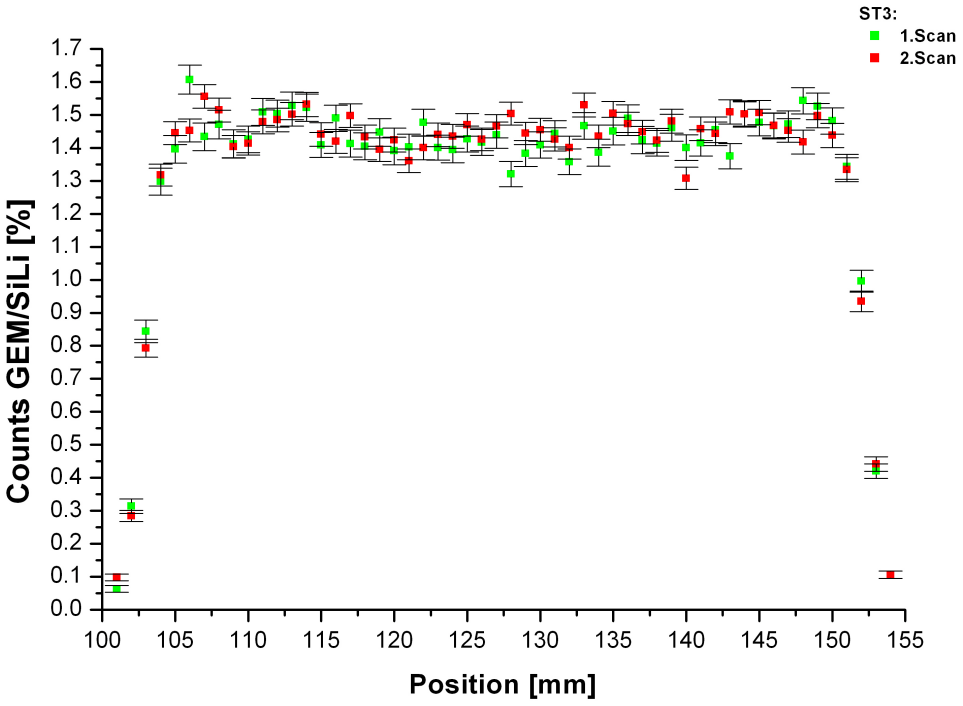


**Figure 4.12:** Both efficiency scans along stripe 3 by comparison

Fig.4.12 shows both measurement runs along stripe 3 by comparison. The constancy confirms the stability of the efficiency along stripe 3.

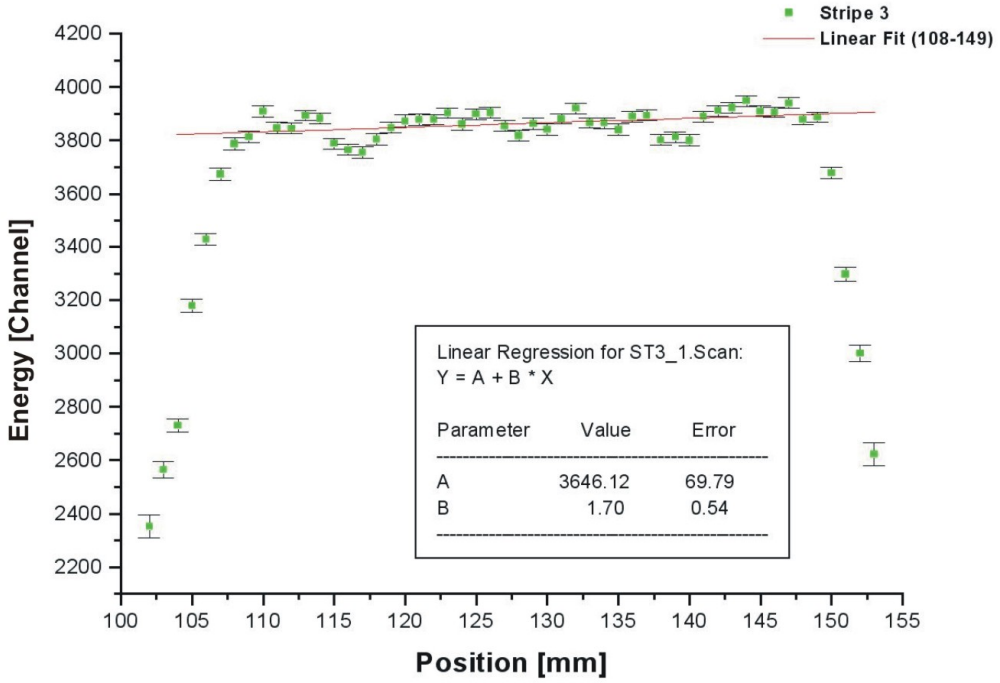


**Figure 4.13:** Comparison of the peak positions of the first measurement run along stripe 3

Fig. 4.13 shows the peak positions during the first measurement run along stripe 3. The full signal height was not achieved at the edges of the stripe. Charge carrier can be lost by edge effects. The signal height of the data points at the inner regions of stripe 3 are nearly equal. Only a few data points around 115 mm and 140 mm are a bit lower but still at the same order.

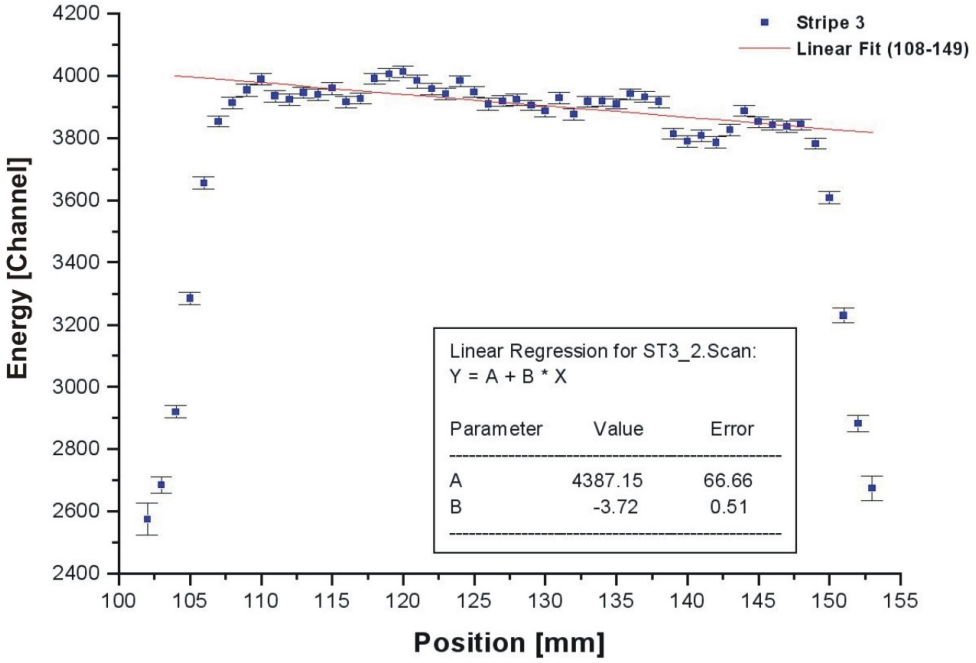


**Figure 4.14:** Comparison of the peak energy of the second measurement run along stripe 3

Fig. 4.14 shows the peak positions during the second measurement run along stripe 3. In contrast to the first measurement a dependence of the peak energy to the position along stripe 3 is clearly recognisable in this graph.

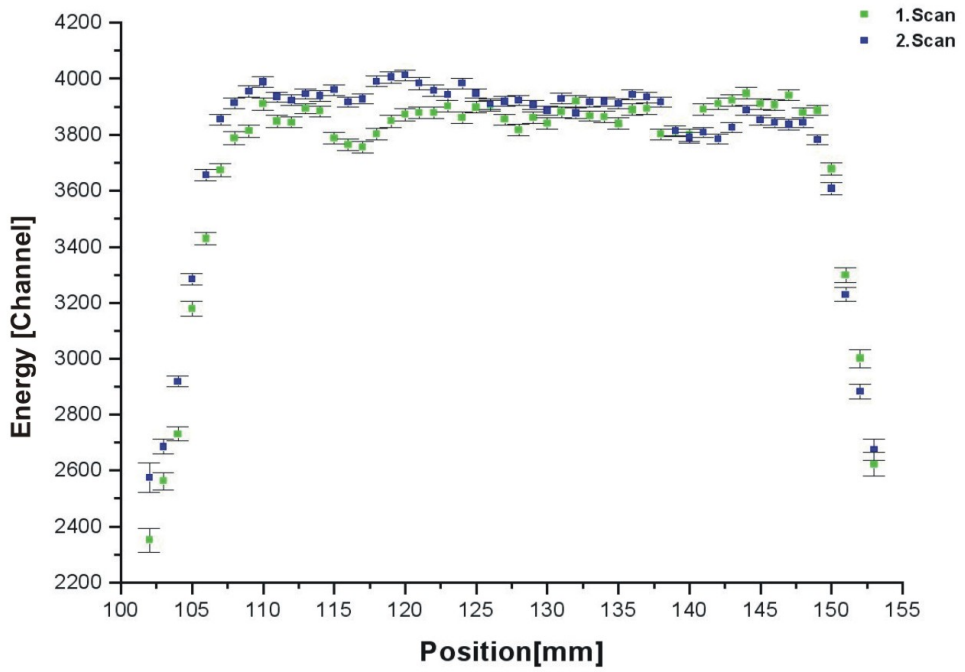


**Figure 4.15:** Both measurement runs along stripe 3 by comparison

At fig. 4.15 the differences between the first and the second measurement run is even more recognisable. It shows, that the data points of both scans are not congruent. Cause the tendency of the peak position at the second scan are not shown in the first scan, it is not possible to make a conclusion relating to the signal amplification along stripe 3.

### 4.2.3 Scan along stripe 4

Similar to stripe 3 the efficiency along stripe 4 shows also a great stability. The data points of the first and second scan are in the same order (see fig. 4.16). The linear fits of fig. 4.17 and fig. 4.18 show constant efficiency and good reproducibility during the first and the second measurement run.

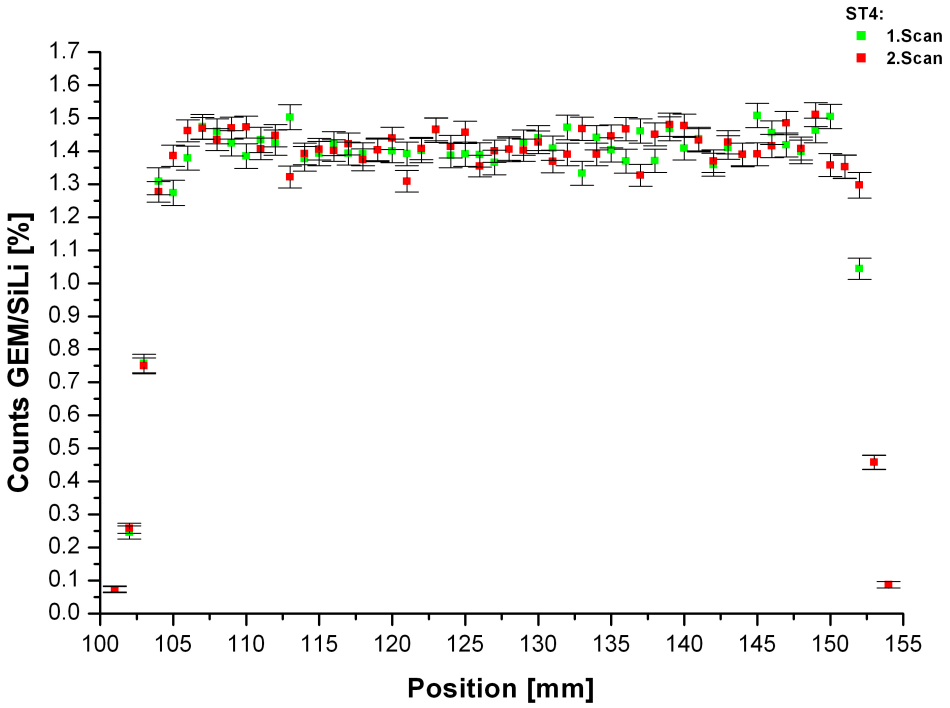


**Figure 4.16:** Both efficiency scans along stripe 4 by comparison

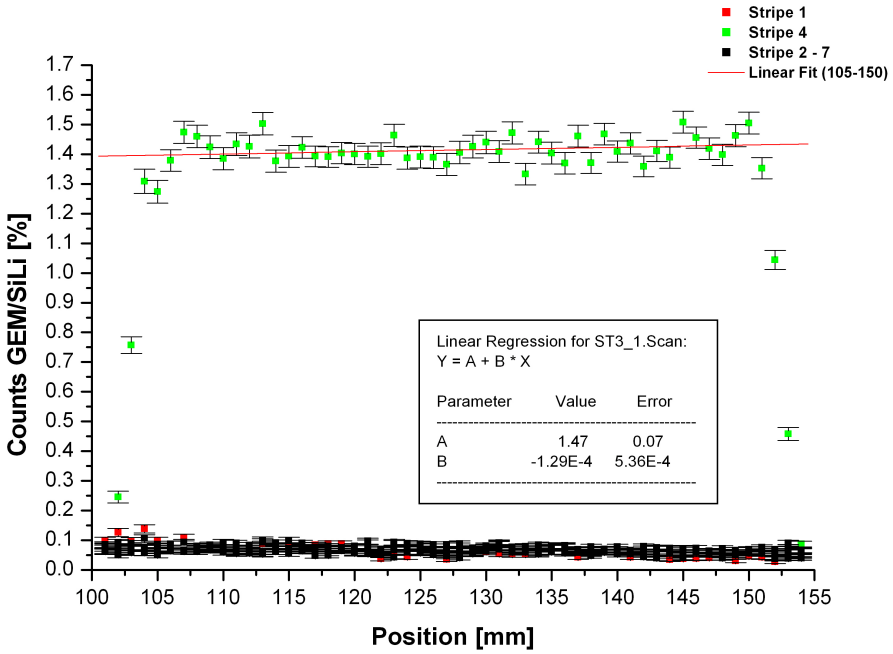


**Figure 4.17:** Number of events of the GEM detector relative to the Si(Li) of the first measurement run along stripe 4.

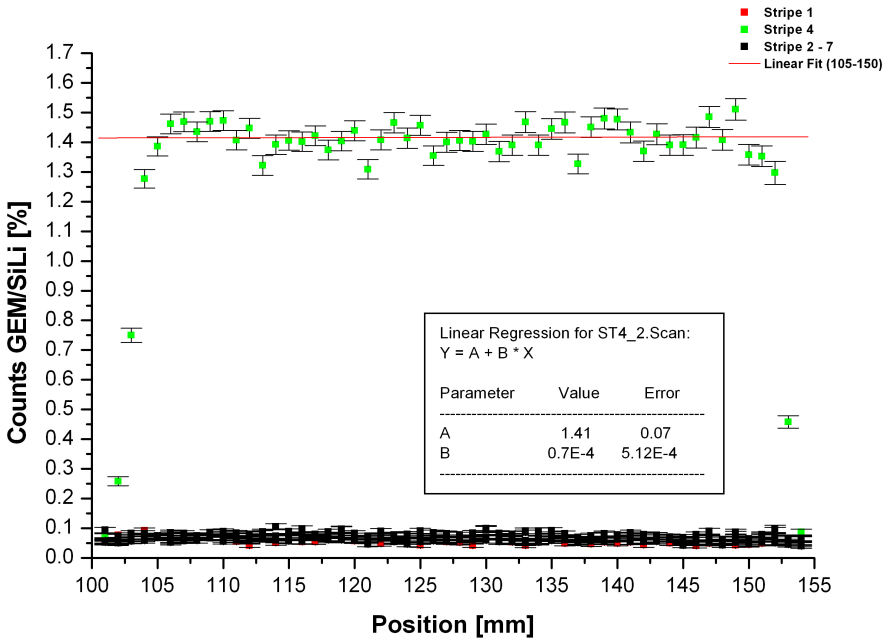


**Figure 4.18:** Number of events of the GEM detector relative to the Si(Li) of the second measurement run along stripe 4.

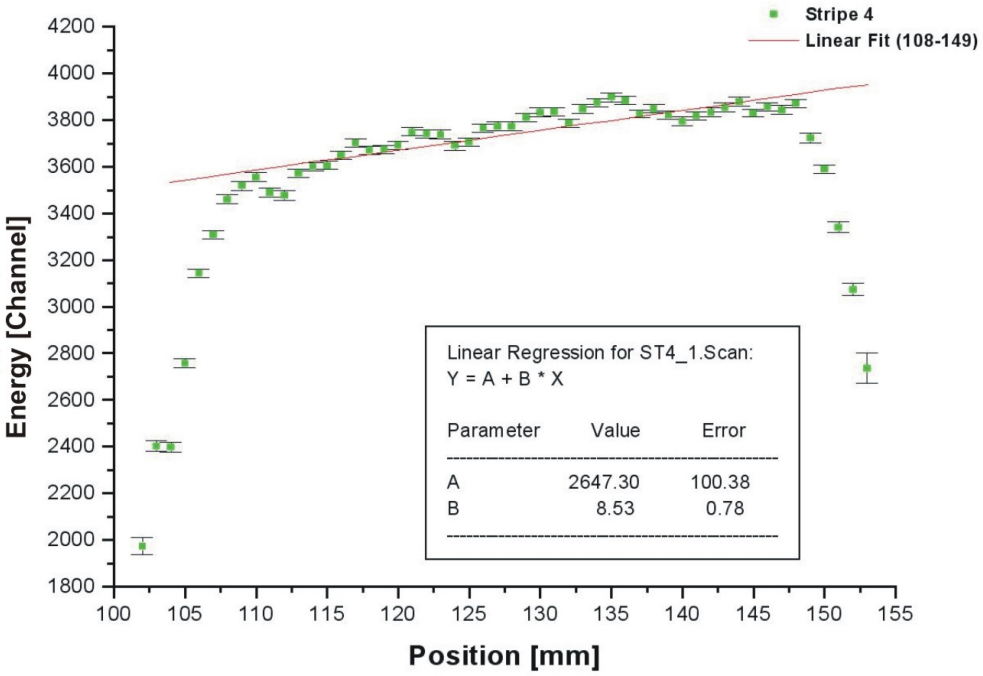


**Figure 4.19:** Comparison of the peak positions of the first measurement run along stripe 4

Fig. 4.19 shows the peak positions during the first measurement run along stripe 4. The dependence of the peak energy to the position along stripe 4 is clearly recognisable in this graph.

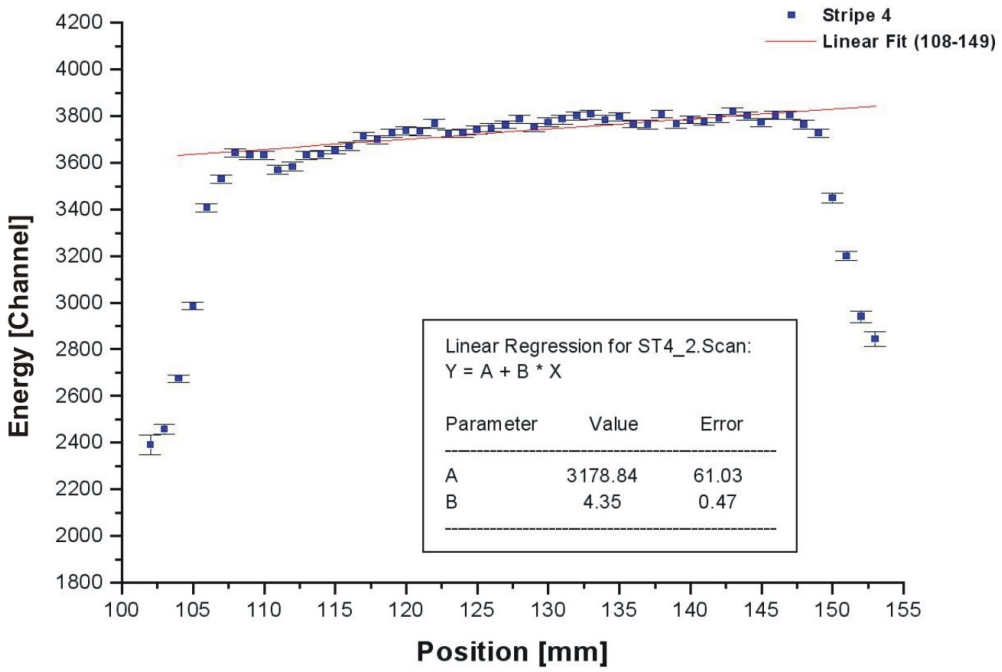


**Figure 4.20:** Comparison of the peak positions of the second measurement run along stripe 4

Fig. 4.20 shows the peak positions during the second measurement run along stripe 4. The position dependence of the peak energy along stripe 4 is also clearly visible in this graph.

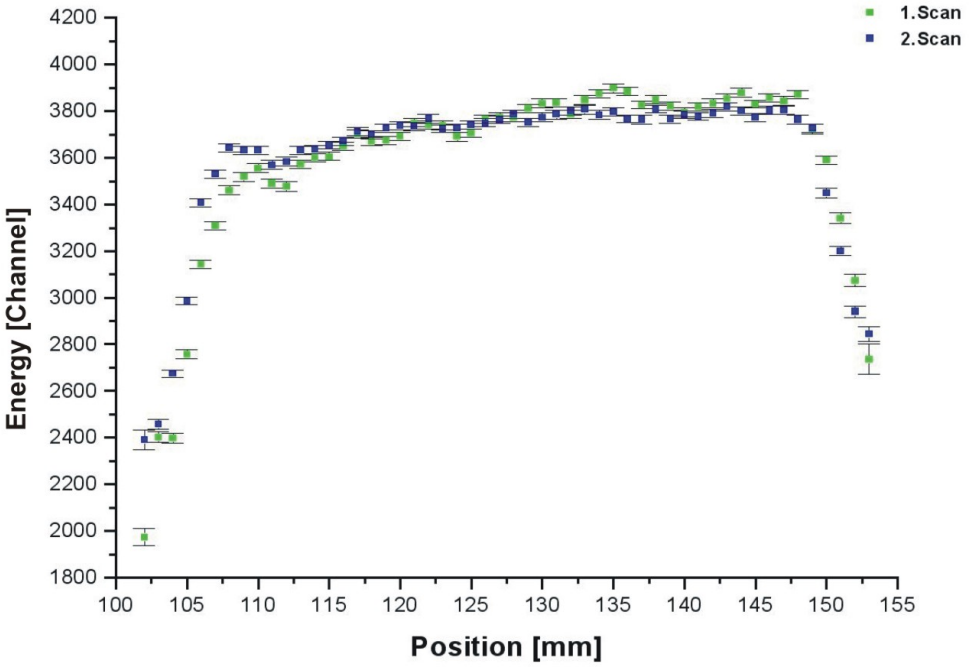


**Figure 4.21:** Both measurement runs along stripe 4 by comparison

Fig. 4.21 shows the peak position along stripe 4 of both measurement runs. By comparison of both measurement runs, the position dependence of the peak energy along stripe 4 is reproducible.

# 5 Discussion and Outlook

## 5.1 Discussion

During this work the location dependence of the intrinsic efficiency and signal amplification across the detection area of a newly developed GEM detector had to be measured. The experiments contained measurement series across all ten stripes of the detection readout and measurement series along two individual stripes (Stripe 3 and stripe 4). All measurement series were performed twice for a check of the consistency.

Four conclusions can be formulated:

- The analyses relating to the efficiency of the measurements series along stripe 3 and stripe 4 show a degree of stability (see subsections 4.2.2 and 4.2.3). Therefore it is assumed that the efficiency along all individual stripes is location-independent.

- The analyses of the measurement series *across* all ten stripes show that the intrinsic efficiencies of all ten stripes are in the same order (see subsection 4.2.1). Time did not allow to perform measurement runs *along* all ten stripes to determine a mean of the efficiency for all ten stripes.

- The amplification along a single stripe is not constant, which becomes obvious from the analyses of the signal amplification along stripe 4 (see subsection 4.2.3). The location-dependence of the peak energy along stripe 4 is clearly an evidence for a diverse signal amplification along stripe 4. The first measurement run along stripe 3 show a location independent signal amplification, but a location dependence during the second run. Further measurements are necessary to provide an insight into possible time-dependent effects.

- The measurement without pinhole between X-ray target and GEM detector shows that the signals of different stripes are differently amplified (see fig. 4.9). The different amplification is mainly given by the preamplifier. A possible effect of the GEM detector assembly could not be determined. A particular discussion about the preamplifier is given in subsection 5.2.2.

## 5.2 Outlook and further Improvements

I want to discuss the problems, which arose during this work, and elaborate further improvements of the GEM detector and the measurement assembly.

### 5.2.1 Low number of events

The biggest problem was the very low number of events (1 - 4 $\#/s$) of the GEM detector during the measurements with the pinhole. Thereby the measurement time had to be at least 300 s to get acceptable statistics for further analyses. That causes a measurement time up to twelve hours for two measurement runs. Because the measurements can not be performed automatically, the measurements had to be observed during the whole experiment. It was not possible to scan the whole detection area of the GEM detector within a measurement week of typically 4 - 5 days.

The low number of events can be improved due to changes of the measurement assembly or modifications of the GEM detector. One of the possible measurement assembly improvements include a reduction of the distance between target and GEM detector. As mentioned in subsection 1.1.3 the in the target produced X-rays suffer an intensity loss by interacting with air on their way to the GEM detector. By decreasing the distance between target and GEM detector the number of detectable X-rays in the GEM detector increases. But the possibility for $H^+$ to reach the detection area of the GEM detector also increases with lesser distance. The gas inside the detector can also be ionised by $H^+$, which will cause additional background events.

The second measurement assembly change could be the use of a pinhole with bigger diameter. Thereby the number of X-rays, which reach the GEM detector will also increase. However by increasing the pinhole diameter the size of the beam spot on the cathode foil will increase. Thereby the size of the excited detection area will also increase, from which it follows that the spatial-resolution of the measurements will become worse.

The active area, where the X-rays should be absorbed and therefore produce a signal in the detector, is between cathode foil and the first GEM foil. An absorption of the X-ray by gas atoms before the cathode foil is useless, because of the applied high voltages the electrons would not be accelerated to the readout anode. A signal, which is produced behind the first GEM foil, has not the full signal high at the readout anode. Due to increased X-ray absorption in matter with increasing thickness of the matter, a larger distance between cathode foil and first GEM foil will be one of the further improvements of the GEM detector.

The second modification regards the readout anode. The readout stripes of the GEM detector were 4 mm broad copper stripes, which are as long as the whole detection area. The spatial resolution exist only in one direction, where it is given by the width of each stripe. It is impossible to differ between the positions of two signals, which hit the same stripe. Therefore one of the biggest improvements of the

GEM detector will be the exchange of the readout anode. The readout anode should be composed of a *grid* of readout stripes. The width of the readout stripes should be only several hundred $\mu m$. Therefore the spatial resolution of the GEM detector will be highly improved. It will be also possible to determine the position of a registered signal in both directions.

Due to this highly improved spatial-resolution, it will be unnecessary to restrict the X-ray beam with a pinhole for further GEM detector measurements to determine a possible location dependence.

### 5.2.2 Preamplifier

As mentioned in subsection 4.2.1 the preamplifier showed different amplification of the signals of different stripes superposing possible effects from the detector itself. For further experiments it is necessary to adapt the preamplifier, so that the amplification of all ten preamplifier channels can be monitored, e.g. by an external calibration pulse.

The preamplifier showed also microphonics during the measurements. The microphonics were observed by an oscilloscope, where the signals of stripe 1 were observed. The higher number of events of stripe 1, caused by the microphonics, is noticeable in fig. 4.10 and fig. 4.11. During the measurements the preamplifier was mounted on the 3-axis computer controlled manipulator nearby the GEM detector. Thus the preamplifier was also moved at each position change. The microphonics became noticeable at the beginning of the measurements. When the manipulator was moved by several cm from a park position to the first measurement point. During the measurement runs the stepsize was only 1 mm. This small position change did not induce microphonics in stripe 1.

Microphonics can be possibly avoided by a separate mounting of the preamplifier.

# Bibliography

C. Altunbas, M. Capèans, K. Dehmelt, J. Ehlers, J. Friedrich, I. Konorov, A. Gandi, S. Kappler, B. Ketzer, R. D. Oliveira, S. Paul, A. Placci, L. Ropelewski, F. Sauli, F. Simon, and M. van Stenis. Construction, test and commissioning ot the triple-gem tracking detector for compass. *Nuclear Instruments and Methods in Physics Research A*, 490:177–203, 2002. 4, 5

F. Eder. Development and evaluation of a pige-setup at vera. Master's thesis, University of Vienna, 2008. 16

Hasberg-Schneider. Technical information, 2000. URL `http://www.hasberg-schneider.de/english/techinfo.html`. 20

H. Krimse. *Transmissionselektronenmikroskopische Untersuchungen von II-VI-Verbindungshalbleitern unterschiedlicher Dimensionierung.* PhD thesis, Humboldt-Universität zu Berlin, 2000. URL `http://edoc.hu-berlin.de/dissertationen/kirmse-holm-2000-12-20/HTML/kirmse-ch4.html`. 2

W. Kutschera. Accelerator mass spectrometry, a versatile tool for research. *Nuclear Instruments and Methods in Physics Research B*, 50:252–261, 1990. 16

W. Kutschera, P. Collon, H. Friedmann, R. Golser, P. Hille, A. Priller, W. Rom, P. Steier, A. Wallner, E. Wild, and G. Winkler. Vera: A new ams-facility in vienna. *Nuclear Instruments and Methods in Physics Research B*, 123:47–50, 1997. 15

P. Milota, I. Reiche, A. Duval, O. Forstner, H. Guicharnaud, W. Kutschera, S. Merchel, A. Priller, M. Schreiner, P. Steier, E. Thobois, A. Wallner, B. Wünschek, and R. Golser. Pixe measurments of renaussance silverpoint drawings at vera. *Nuclear Instruments and Methods in Physics Research B*, 266:2279–2285, 2008. 16, 17

F. Murtas. Development of a gaseous detector based on gas electron multiplier (gem) technology. Talk at Frascati, November 2002. Private Communication with Dr. Johann Zmeskal (SMI, Vienna). 5

A. Priller, R. Golser, P.Hille, W. Kutschera, W. Rom, P. Steier, A. Wallner, and E. Wild. First performance test of vera. *Nuclear Instruments and Methods in Physics Research B*, 123:193–198, 1997. 15

A. Priller, R. Golser, W. Kutschera, P. Steier, C. Vockenhuber, and S. Winkler. Upgrade of the analyzing beamline at the vera labratory. In R. e. a. Hellbourg, editor, *Proceedingsot the 34th SymposiumNorth Eastern Accelerator Personnel, Lund, Sweden*, pages 68–80. World Scintific Publishing Co., 2002. 15

G. Rech, J. Lee, E. B. Norman, R.-M. Larimer, and L. Guthrie. Viewing the periodic table of the elements with x-ray. URL `http://ie.lbl.gov/xray/`. 3

L. Reichhart. Depth-resolved pixe analysiswith a polycapillary x-ray lens. Master's thesis, University of Vienna, 2008. 16

P. Steier, R. Golser, W. Kutschera, A. Priller, C. Vockenhuber, and S. Winkler. Vera, an ams facility for "all" isotopes. *Nuclear Instruments and Methods in Physics Research B*, 223-224:67–71, 2004. 15

A. Thompson, D. Attwood, E. Gullikson, M. Howells, K.-J. Kim, J. Kirz, J. Kortright, I. Lindau, P. Pianetta, A. Robinson, J. Scofield, J. Underwood, D. Vaughan, G. Williams, and H. Winick. X-ray data booklet, center for x-ray optics and advanced light source, January 2001. 24

# List of Figures

# List of Tables

# Acknowledgments

At first I want to thank Walter Kutschera and Robin Golser for giving me the opportunity to do my diploma thesis at VERA. Furthermore I want to thank:

Especially, Johann Zmeskal from the SMI for supervising me during the work and for his general support

Herbert Schneider from the SMI for the electrical composition of the GEM detector and his help during the first measurments

Tomoichi Ischiwatari from the SMI for his help with the data analysis and the configuration of the signal processing assembly

Ewald Friedl, Johann Lukas, Wolfgang Hieß and Gabi Obstmayer for their fast and precise work

Alfred Priller, Peter Steier, Anton Wallner and Oliver Forstner for their help with tunning the accelerator and the immediately reparations in case of technical emergencies

Lea Reichhart, Fabiennen Eder and Daniel Imrich for their help during the measurements and for keeping me company during long measurement days

Furthermore, I want to thank my parents for their mental and financial support and my girlfriend Conny for her patience, understanding and encouraging words.

# Curriculum vitae

**Name: Philipp Müllner**

**Date of birth:** December $13^{th}$, 1982

**Place of birth:** Krems

**Nationality:** Austria

**Marital status:** single

**1993-2001:** Bundesrealgymnasium , Krems
Matura on 6/6/01

**September 2001–April 2002:** Mandatory military service in Mautern, NÖ

**since 2002:** Diploma study of physics at the University of Vienna

**since october 2007:** Diploma thesis at VERA, Isotopenforschung, Fakultät für Physik, University of Vienna with the title: *Characterisation of a new GEM-detector with PIXE at VERA* (supervisor: Ao. Univ.-Prof. DI Dr. Robin Golser, co-supervisor: Dr. Johann Zmeskal)

# Lebenslauf

**Name: Philipp Müllner**

**Geburtsdatum:** 13. Dezember 1982

**Geburtsort:** Krems

**Staatsbürgerschaft:** Österreich

**Familienstand:** ledig

**1993-2001:** Bundesrealgymnasium, Krems
Matura am 06.06.2001

**September 2001–April 2002:** Präsenzdienst in Mautern, NÖ

**seit 2002:** Diplomstudium Physik an der Universität Wien

**seit Oktober 2007:** Diplomarbeit bei VERA, Isotopenforschung, Fakultät für Physik, Universität Wien mit dem Thema: *Characterisation of a new GEM-detector with PIXE at VERA* (Betreuung: Ao. Univ.-Prof. DI Dr. Robin Golser, Dr. Johann Zmeskal)